Title: Functional analyses of extracellular cysteine residues and phosphorylation for immune responses mediated by the *Arabidopsis* cysteine-rich receptor-like kinase CRK28

Authors: Koste A. Yadeta[1], James M. Elmore[1,2], Athena Y. Creer[1], Baomin Feng[4], Jessica Y. Franco[1], Jose Sebastian Rufian[3], Ping He[4], Brett Phinney[5], Gitta Coaker[1*]

Affiliations:

[1]Department of Plant Pathology, University of California Davis, Davis, California, 95616, USA

[2]Current address: Corn Insects and Crop Genetics Research Unit, U.S. Department of Agriculture-Agricultural Research Service, Iowa State University, Ames, IA, USA

[3] Current address: Instituto de Hortofruticultura Subtropical y Mediterránea "La Mayora" – Universidad de Málaga – Consejo Superior de Investigaciones Científicas, Campus de Teatinos s/n, Málaga E-29071, Spain

[4]Department of Biochemistry and Biophysics, and Institute for Plant Genomics & Biotechnology, Texas A&M University, College Station, Texas, United States of America

[5]Genome Center Proteomics Core Facility, University of California Davis, Davis, California, 95616, USA

[*]Address correspondence to: glcoaker@ucdavis.edu

Running title: Structure function analyses of CRK28

Abstract

Membrane localized proteins perceive and respond to biotic and abiotic stresses. We performed quantitative plasma membrane proteomics in the model plant *Arabidopsis thaliana* after bacterial elicitor flagellin perception. Over 3,500 proteins were quantified including 404 receptor-like kinases (RLKs). We identified multiple cysteine-rich receptor-like kinases (CRKs) that are upregulated upon perception of flagellin. CRKs possess extracellular cysteine-rich domains and comprise a large gene family consisting of 46 members in *Arabidopsis.* Single T-DNA insertion lines in *CRK28* and *CRK29,* two CRKs induced in response to flagellin perception, did not exhibit robust alterations in immune responses. In contrast, silencing multiple induced CRKs resulted in enhanced susceptibility to pathogenic *Pseudomonas syringae*, indicating functional redundancy in this large gene family. *CRK28* and *CRK29*'s transcripts were barely detectable at a resting state but were strongly induced upon pathogen perception. *Arabidopsis* lines with enhanced expression of *CRK28* exhibited a stronger reactive oxygen species (ROS) burst in response to bacterial flagellin and enhanced resistance to *P. syringae*. Transient expression of a subset of CRKs in *N. benthamiana*, including CRK28, induced cell death. The extracellular cysteine residues predicted to form disulfide bonds were required for cell death induction. CRK28 co-immunoprecipitated with the common RLK co-receptor BAK1 and was present in the FLS2/BAK1 immune complex upon flagellin perception. Silencing the *N. benthamiana BAK1* homologue significantly compromised CRK28-induced cell death. Co-immunoprecipitation assays revealed that CRK28 self-associates and associates with the closely related CRK29.

47 CRK28 was phosphorylated *in planta* and phosphorylation was required for cell death induction.
48 Taken together, these data indicate that subsets of *Arabidopsis* CRKs coordinately function to
49 enhance plant immune responses.
50

Author Summary

In order to resist infection by pathogenic microbes, plants rely on physical barriers, preformed defenses, as well as innate immune receptors that actively recognize pathogen components. Many plant immune receptors are receptor-like kinases (RLKs). The *Arabidopsis* FLAGELLIN-SENSING2 (FLS2) RLK recognizes bacterial flagellin and is one of the best characterized immune receptors. Using a proteomics approach, we detected dynamic changes in the *Arabidopsis* membrane proteome upon flagellin perception and identified multiple cysteine-rich RLKs (CRKs) that were strongly expressed after initial immune perception. Silencing pathogen-induced *CRKs* resulted in enhanced susceptibility to bacterial infection. Subsequent experiments focused on CRK28 and enhanced expression of CRK28 induced plant defense responses. CRK28-mediated defense responses required the common RLK co-receptor BAK1. CRK28 associated with BAK1 as well as the activated FLS2 immune receptor complex. CRK28 self-associated as well as associated with the closely related CRK29. Collectively, these results indicate that suites of CRKs are induced upon pathogen infection and function to enhance plant defense responses.

Introduction

Plants are in close contact with a variety of microorganisms, including pathogens. Plants possess physical barriers to pathogen ingress, including a waxy cuticle and cell wall. There are also large numbers of germline encoded extra- and intracellular innate immune receptors that actively perceive pathogens and induce cellular reprogramming for defense (1, 2). Surface localized receptors with extracellular domains can perceive conserved pathogen/microbe-associated molecular patterns (PAMPs/MAMPs), such as bacterial flagellin or fungal chitin, and induce pattern-triggered immunity (PTI) (1). PTI responses include Ca^{2+} influx, an extracellular reactive oxygen species (ROS) burst, activation of mitogen-activated protein kinases (MAPKs), transcriptional reprogramming, and callose deposition (3). While Ca^{2+} influx, the oxidative burst, and MAPK activation occur within minutes of PAMP perception, callose deposition is a later response occurring several hours post-perception (3). Thus, adapted pathogens must overcome PTI in order to grow and to cause disease. A common mechanism for PTI suppression is the secretion of pathogen proteins, called effectors, into the apoplast or inside host (4, 5). Plants can also recognize specific intracellular pathogen effectors using resistance proteins and induce effector-triggered immunity (ETI) (2). Although there is significant overlap in PTI and ETI based responses, ETI typically induces a stronger response and culminates in programmed cell death at the site of infection (2).

PTI receptors are receptor-like kinases (RLKs) or receptor-like proteins (RLPs) possessing extracellular ligand binding domains (1). The *Arabidopsis* FLAGELLIN-SENSING 2 (FLS2) is a well-studied RLK and perceives a 22-amino acid epitope of bacterial flagellin called flg22 (6).

Upon flg22 perception, FLS2 rapidly heterodimerizes with its RLK co-receptor BAK1 and its closest homolog SERK4 leading to the activation of PTI responses (7-9). *BAK1,* also known as *SERK3*, is a member of the somatic embryogenesis-related kinase (*SERK*) family. BAK1 also heterodimerizes with other immune- related RLKs and RLPs in a ligand-dependent manner (10). Some immune receptors require additional SERK family members for defense signaling (9). Thus, members of the SERK family play crucial roles in plant immunity.

RLKs can function in development, defense, and abiotic stress responses (1, 11, 12). Cysteine-rich receptor-like kinases (CRKs) are a large subfamily of *Arabidopsis* RLKs. Like most RLKs, CRKs possess an extracellular domain, a single-pass transmembrane domain, and an intracellular Serine/Threonine (Ser/Thr) protein kinase domain (13). In their extracellular domain, most CRKs possess two copies of domain of unknown function 26 (DUF26). The DUF26 domain possesses a conserved C-X_8-C-X_2-C motif (13, 14). The cysteine residues in each DUF26 domain are predicted to form two cysteine bridges, which are hypothesized to be targeted for apoplastic redox modification (15). In the *Arabidopsis* genome, there are 46 predicted *CRKs*, eight plasmodesmata-located proteins (PDLPs) and more than 50 cysteine-rich repeat secretory proteins (CRRSP) that possess DUF26 domains (13, 15, 16). PDLPs are RLPs with similarity to CRK extracellular domains (13). PDLPs are involved in the regulation of plant cell-to-cell communication, viral cell-to-cell movement, and plant immunity (16-18).

Previous studies have demonstrated that *Arabidopsis CRKs* are transcriptionally induced in response to abiotic stresses including salicylic acid, ozone, UV, salt, and drought treatments (15, 19-22). A subset of CRKs is strongly induced in response to pathogens and PAMP treatment (15,

21). The coordinated transcriptional induction of CRKs during immune responses suggests that they cooperate to enhance defense signaling. Recently, large-scale phenotyping of T-DNA knockout lines for 41 *Arabidopsis CRKs* has been performed (15). Individual T-DNA knockout lines in most *CRKs* lack strong immune related phenotypes (15). In contrast, overexpression of some *CRKs* robustly enhances plant immune responses. Overexpression of *CRK4*, *CRK5*, *CRK6*, *CRK13*, and *CRK36* in *Arabidopsis* resulted in enhanced resistance to the bacterial pathogen *Pseudomonas syringae* pv. *tomato* (*Pst*) (19, 22, 23). Furthermore, overexpression of *CRK4*, *CRK6* and *CRK36* enhanced the activation of early and late PTI responses (22). Overexpression of *CRK4*, *CRK5*, *CRK13*, *CRK19*, and *CRK20* in *Arabidopsis* also induces cell death (19, 23).

A mechanistic understanding of CRK function for plant immune responses, including the identification of CRK interacting proteins, the role of the extracellular cysteine residues, and the importance of kinase activity remains largely unknown. Quantitative proteomics analyses were performed upon perception of flg22, identifying multiple CRKs whose protein abundance is significantly increased. Here, we report the functional characterization of *CRK28* in plant immunity. Overexpression of *CRK28* in *Arabidopsis* enhanced resistance to *Pst*. Transient expression of *CRK28* in *N. benthamiana* induced cell death. CRK28's extracellular cysteine residues and the conserved lysine in its kinase domain are required for cell death induction. Furthermore, we show that CRK28 associates with BAK1 and is present in the FLS2-BAK1 immune complex. Lastly, using immunoprecipitation, we demonstrated that CRK28 self-associates and also associates with the closely related CRK29.

Results

Quantitative proteomics identifies multiple receptor-like kinases induced upon flagellin perception

In order to identify proteins whose levels dynamically change upon perception of flg22, four-week-old *Arabidopsis* plants were sprayed with 10μM flg22 peptide or water. Rosette tissue was harvested at 180min and 720min for plasma membrane enrichment followed by liquid chromatography tandem mass spectrometry (LC-MS/MS) analyses (Fig 1A). Proteins with more than one spectral count in at least two of the three biological replicates were used for differential abundance analyses. The intersection of two statistical frameworks (QPROT and edgeR) was used to detect proteins exhibiting differential abundance (24, 25). A total of 3,589 proteins were reproducibly identified revealing multiple classes of differentially expressed proteins known to be involved in immune signaling such as: protein phosphatases, calcium signaling, protein kinases, and RLKs (S1 Table, Fig 1B).

Fig 1. Plasma membrane proteomics identified multiple differentially expressed RLKs upon perception of bacterial flagellin.

We reproducibly identified 404 RLKs by MS/MS, representing almost two-thirds of all RLKs encoded in the *Arabidopsis thaliana* genome. Furthermore, 49 of the identified RLKs were differentially expressed over the course of the experiment (Fig 1C). The RLK subfamily was divided into leucine-rich repeat (LRR) and non-LRR RLKs and phylogenetic trees were constructed based on their kinase domain sequences (S1-2 Fig) (26). Differential protein abundance of LRR-RLKs was primarily detected in the LRR-Ia and LRR-XI subfamilies (Fig 1C, S1 Fig). Several LRR-XI subfamily members with known or putative roles in development were

down-regulated (eg. BARELY ANY MERISTEM 1/2 (BAM1/2), HAESA-LIKE 1 (HSL1), the *Arabidopsis* C-TERMINALLY ENCODED PEPTIDE RECEPTOR 2 (CEPR2)) (27-29), consistent with the antagonism between plant growth and defense. The immune receptors ELONGATION FACTOR TU RECEPTOR (EFR) and FLS2 were also upregulated at 720min (Fig 1C, S1 Fig). EFR is the *Arabidopsis* receptor for the bacterial PAMP elongation factor Tu (30). Activated FLS2 is ubiquitinated and endocytosed after perception of flg22 (31, 32). However, after FLS2 degradation occurring ~1h post-flg22 perception, *de novo* protein synthesis results in an increase in FLS2 protein levels between 3-24h post-perception, which is consistent with our results (33). The major chitin receptor LYSIN MOTIF RECEPTOR KINASE5 (LYK5) (34), the lipopolysaccharide receptor LECTIN S-DOMAIN-1 RECEPTOR-LIKE KINASE (LORE) (35), the damage associated molecular pattern receptor WALL-ASSOCIATED RECEPTOR KINASE 1 (WAK1) (36), and the danger peptide receptor PEP RECEPTOR 1 (PEPR1) (12) were upregulated upon flg22 perception (Fig 1C, S1 Fig, S2 Fig). These results indicate that additional RLKs are induced to enhance immune responses or pathogen detection after initial flg22 perception.

We also detected an increase in abundance of six CRKs upon flg22 perception (CRK11, 13, 13, 22, 28, 29) (Fig 1C, S2 Fig). In the *Arabidopsis* genome, 40 of the 46 predicted *CRKs* are located on chromosome 4, with the largest cluster comprising 20 *CRKs* in a tandem array (S3 Fig). To investigate transcript expression of *CRKs* during plant immune responses, we mined available *Arabidopsis* expression data generated upon treatment with the bacterial pathogen *Pst*, the bacterial PAMPs flg22 and elf26, as well as fungal chitin. Elf26 is an immunogenic 26 amino acid epitope of the bacterial PAMP elongation factor Tu (37). Treatment with *Pst,* flg22, or elf26

strongly induces the transcription of most *CRKs* on chromosome 4 (Fig 1D). Taken together, these data demonstrate that *CRKs* are highly expressed upon PAMP perception, suggesting that multiple *CRKs* are collectively involved in plant immune responses.

Genetic analyses of CRK-mediated defense

We investigated the expression levels of *CRK28* (At4g21400) and *CRK29* (At4g21410), two closely related *CRKs* that are induced upon PTI perception in our proteomics analyses. In order to investigate their transcriptional regulation, four-week-old Col-0 plants were sprayed with either flg22 or water and leaf samples were subjected to quantitative real-time PCR (qPCR) analyses. Both *CRK28* and *CRK29* were strongly induced 3h post-flg22 elicitation (~18 fold) compared to water treatment (Fig 2A). We obtained T-DNA insertion lines for *CRK28* (*crk28-1*) and *CRK29* (*crk29-1*) (S4A Fig). While *crk29-1* is a true knockout, *crk28-1* is a knockdown (S4B-C Fig). *crk28-1* and *crk29-1* were challenged by syringe infiltration with the virulent *Pst* or spray inoculated with *Pst* Δ*hrcC*, which is unable to deliver effectors, but we did not observe a significant difference in bacterial titer between the mutants and Col-0 (S4D, S4E Fig). Flg22 pretreatment protects *Arabidopsis* plants from subsequent infection by virulent *Pst* (38). We did not observe a significant difference in flg22-mediated protection in *crk28-1* and *crk29-1* compared to Col-0 (S4F Fig).

To investigate the cumulative role of pathogen-responsive CRKs, we silenced *CRK22* and *CRK28* in the *crk29-1* knockout using virus induced gene silencing (VIGS, Fig 2B-C). Plants silenced with *CLA1* (*cloroplastos alterados* 1) exhibited an albino phenotype and were used as a visual marker for VIGS efficiency (Fig 2B). Wild-type Col-0 plants silenced with VIGS

constructs containing *GFP* or *crk29-1* plants silenced for *CRK22* and *CRK28* did not exhibit alterations in plant growth (Fig 2B). RT-PCR demonstrated silencing of *CRK22* and *CRK28* in *crk29-1* lines, but not *CRK13* (Fig 2C). As has been previously reported, silencing *Arabidopsis* Col-0 plants with VIGS constructs containing *GFP* does not affect *Pst* growth (Fig 2D) (39). Silencing of *CRK22* and *CRK28* in the *crk29-1* knockout resulted in significantly higher bacterial titers compared to Col-0 control plants three days post-inoculation (Fig 2D). These data indicate that pathogen-induced CRKs are important in inhibiting bacterial growth.

Fig 2. Genetic investigation of CRK-mediated responses to *Pseudomonas syringae.*

Increased expression of CRK28 enhances resistance to *Pseudomonas syringae*

Transgenic lines were generated expressing *CRK28* genomic DNA under the control of its native promoter with a C-terminal fusion to the 3XFLAG epitope (*npro:CRK28-FLAG*) in the *crk28-1* background. Two independent T3 homozygous lines (28-1 and 28-2) were obtained. Anti-FLAG immunoblotting revealed that CRK28 expression in *npro:CRK28-FLAG* line 28-1 is significantly lower than in line 28-2 (Fig 2E). Quantitative PCR analyses revealed that both *npro:CRK28-FLAG* lines exhibited significantly higher *CRK28* transcript accumulation than Col-0 (Fig 2F). No obvious developmental phenotypes were observed in *npro:CRK28-FLAG* lines. The *npro:CRK28-FLAG* lines were infiltrated with *Pst* strain DC3000 and disease progression was monitored over time. Col-0 exhibited strong disease symptoms, whereas *npro:CRK28-FLAG* lines did not display any obvious *Pst* symptoms four days post-infiltration (dpi) (Fig 2G).

Quantification of the bacterial titers correlated with visual disease symptoms. Col-0 harbored significantly higher bacterial titers than *npro:CRK28-FLAG* lines 28-1 and 28-2 (Fig 2H). Bacterial titers negatively correlated with the level of *CRK28* expression, *npro:CRK28-FLAG* line 28-2 exhibited ~10 fold lower bacterial growth and line 28-1 exhibited ~5 fold lower bacterial growth than Col-0 (Fig 2). Taken together, these results demonstrate that *CRK28* is rapidly induced upon PAMP perception and the level of expression correlates with the heighted resistance to *Pst.*

Extracellular cysteine-residues are required for CRK28-induced cell death in *N. benthamiana*

Previous studies have demonstrated that overexpression of *CRK4*, *CRK5*, *CRK13*, *CRK19* and *CRK20* in *Arabidopsis* induce cell death (19, 20, 23). In order to identify a strong CRK-related phenotype for functional analyses, we investigated the ability of *CRK13*, *CRK28*, and *CRK29* to elicit cell death upon transient expression in *Nicotiana benthamiana*. *CRK13* was included as a control because overexpression in *Arabidopsis* has been previously shown to induce cell death (23). When transiently expressed in *N. benthamiana, 35S:CRK13-FLAG*, *35S:CRK28-FLAG*, and *35S:CRK29-FLAG* elicited cell death 24 hours post-inoculation (hpi) (Fig 3B). Leaves infiltrated with the negative control *35S:GFP* did not exhibit cell death (Fig 3B). Expression of *35S:CRK28-FLAG* and *35S:CRK29-FLAG* induced stronger and faster cell death than expression of *35S:CRK13-FLAG* (Fig 3B). Using anti-FLAG immunoblotting, all three constructs were expressed in *N. benthamiana* (Fig 3C). *CRK28* and *CRK29* are closely related, strongly induced in response to PAMP treatment, and elicit similar phenotypes when expressed in *N. benthamiana*

(Fig 1-3). Therefore, we focused on investigating *CRK28* in subsequent experiments. When amplifying cDNA corresponding to *CRK28*'s transcript, we found that it does not match the gene model present in The Arabidopsis Information Resource (TAIR) database and contains seven exons (S4A, S5 Fig).

Fig 3. CRK28's extracellular cysteine residues are required for cell death induction in *Nicotiana benthamiana*.

In both *Arabidopsis* and *N. benthamiana* CRK28 was detected at molecular weight of ~100kDa by Western blotting (Fig 2E, 3C). However, CRK28's molecular weight is predicted to be 74.46kDa. Similarly, CRK13 and CRK29 also ran higher than their predicted molecular weight of 75.29kDa and 75.72kDa, respectively (Fig 3C). Other transmembrane proteins such as FLS2 and EFR also run larger than their predicted molecular weight due to complex *N*-linked glycosylation (40, 41). Incubation of CRK28 protein extract from *N. benthamiana* with both *N*-linked glycosylases PNGase F and EndoHf resulted in the detection of some of CRK28 at its predicted molecular weight (Fig 3F). A significant amount of CRK28 was resistant to glycosylase treatment likely due to either incomplete digestion or the presence of more complex *N*-linked glycans. *N*-glycosylation is further modified in the golgi apparatus by the addition of β (1,2)-xylose or α (1,3)-fucose (42). These complex *N*-linked glycans are often resistant to a single enzymatic digestion. To investigate if CRK28 carries complex *N*-linked glycans, we transiently expressed *35S:CRK28-FLAG* and *35S:GFP* in *N. benthamiana* and performed anti-FLAG immunoprecipitation. Anti-HRP antibody has previously been used to detect complex *N*-linked glycans (42). Anti-HRP immunoblotting showed that in addition to endoplasmic reticulum

(ER) *N*-glycosylation CRK28 is further glycosylated in the golgi (Fig 3G). Together, these results show that CRK28 is a complex glycosylated transmembrane protein.

The majority of the *Arabidopsis* CRKs possess two copies of DUF26 in their extracellular region. The four cysteine residues in each DUF26 domain are predicted to form two cysteine bridges (Fig 3A). Disulfide bonds are ROS sensitive and are important for protein folding, structure, and stability (43-45). Thus, we investigated the role of extracellular cysteine residues predicted to be involved in disulfide bond formation for CRK28-mediated cell death induction in *N. benthamiana*. Cysteine bridges were disrupted by mutating one cysteine residue from each pair into alanine. Wild-type *CRK28* (*35S:CRK28-FLAG*) and the cysteine mutants (*35S:CRK28^{C99A}-FLAG*, *35S:CRK28^{C127A}-FLAG*, *35S:CRK28^{C214A}-FLAG*, and *35S:CRK28^{C242A}-FLAG*) were transiently expressed in *N. benthamiana* using *Agrobacterium*. As expected, *N. benthamiana* leaves infiltrated with *35S:CRK28-FLAG* exhibited cell death starting at 18hpi (Fig 3D). However, none of the cysteine mutants induced cell death (Fig 3D), suggesting that the extracellular cysteine residues are required for cell death induction. Mutating the cysteine residues did not affect protein stability as all the cysteine mutants were expressed to the same level as the wild type by anti-FLAG immunoblotting (Fig 3E).

CRK28's kinase active site is required for function in *Nicotiana benthamiana* and *Arabidopsis*

CRKs possess a serine/threonine (Ser/Thr) kinase domain with all the predicted consensus features (Fig 3A) (46). However, it is still unknown whether kinase activity is required for CRK

function or if CRKs are phosphorylated *in planta*. We tested the importance of CRK28's active site for inducing cell death in *N. benthamiana*. The highly conserved lysine (K377) residue in CRK28's ATP binding motif was mutated to asparagine (N) (*35S:CRK28^{K377N}-FLAG*). Mutating this conserved lysine residue in Ser/Thr protein kinases has previously been shown to block activity (47, 48). None of the leaves infiltrated with *35S:CRK28^{K377N}-FLAG* exhibited cell death, but all leaves infiltrated with wild-type *35S:CRK28-FLAG* exhibited cell death (Fig 4A). Anti-FLAG immunoblotting demonstrated equal expression of CRK28-FLAG and CRK28^{K377N}-FLAG (Fig 4B). Overall, these results suggest that the invariant lysine residue is required for CRK28-induced cell death.

Fig 4. The CRK28 intracellular ATP binding lysine (K377) residue is required for CRK28-mediated function and CRK28 is phosphorylated *in planta*

The kinase domain of CRK28 and CRK28^{K377N} were expressed in *E. coli* as MBP fusion proteins. However, no kinase activity was detected with recombinant proteins (S6 Fig). However, kinase activity was observed for the positive control RIPK (49). To investigate if CRK28 is phosphorylated *in planta,* CRK28-FLAG, CRK28^{K377N}-FLAG and GFP were expressed in *N. benthamiana* and immunoprecipitated using anti-FLAG agarose beads. Subsequently, the IP was used for anti-phospho immunoblotting and radioactive ^{32}P based kinase activity assays. We did not detect CRK28 kinase activity using radioactivity assays after immunoprecipitation (IP) *in planta*. However, we were able to detect phosphorylation of wild-type CRK28, but not CRK28^{K377N} using anti-phospho immunoblotting after IP (Fig 4C). Thus, CRK28 is phosphorylated *in planta.*

The importance of CRK28's conserved lysine residue was also investigated in *Arabidopsis*. *35S:CRK28-FLAG* and *35S:CRK28^{K377N}-FLAG* constructs were transformed into Col-0. Few transformants were obtained from Col-0 transformed with *35S:CRK28-FLAG* compared to *35S:CRK28^{K377N}-FLAG*. Furthermore, the surviving *35S:CRK28-FLAG* T1 transgenics exhibited shorter stature, increased inflorescence branch numbers, shorter siliques, and a lack of seed set (Fig 4D). Plants transformed with *35S:CRK28^{K377N}-FLAG* exhibited wild-type growth (Fig 4D). Protein expression levels were similar between CRK28-FLAG and CRK28^{K377N}-FLAG transformants (Fig 4E), further confirming that an intact kinase domain is required for the phenotypes observed.

CRK28 expression is induced in response to flg22 and enhances the extracellular ROS burst

There is a positive correlation between *CRK28*'s basal expression level and resistance to *Pst* in *npro:CRK28-FLAG* transgenic lines (Fig 2). In order to investigate the expression of *CRK28* in Col-0 and *npro:CRK28-FLAG* transgenic lines, we treated with 10µM flg22 or water and leaf samples were collected at 0 and 3hrs post treatment for qPCR. *CRK28* transcripts were strongly induced in response to flg22 treatment and significantly higher in *npro:CRK28-FLAG* 28-1 and 28-2 lines compared to Col-0 (Fig 5A). We also observed that water treatment increased the expression of *CRK28*, but this was more pronounced and statistically significant in the highest expressing line (Fig 5A). The flg22-triggered increase of *CRK28* expression was more pronounced in *npro:CRK28-FLAG* line 28-2, which exhibits the highest basal expression of *CRK28,* compared to line 28-1 (Fig 5A).

Fig 5. CRK28 expression is induced in response to flg22 and heighted expression of CRK28 enhances flg22-triggered ROS burst.

Next, we examined the induction of the extracellular ROS burst and MAPK activation, two common PTI markers (3). To measure the ROS burst, two-week-old Col-0, *npro:CRK28-FLAG* line 28-1 and line 28-2 were treated with flg22 and the fungal elicitor chitin. While flg22 treatment significantly increased ROS accumulation in *npro:CRK28-FLAG* 28-1 and 28-2 lines compared to Col-0, treatment with chitin did not alter ROS accumulation (Fig 5B-C). Consistent with this observation, transcript analyses of *CRK* expression upon elicitor treatment revealed that many *CRK*s, including *CRK28*, are induced upon flg22 treatment (Fig 1D). In contrast, fewer *CRKs* are induced in response to chitin treatment (Fig 1D). We also examined if MAPK activation is altered in *npro:CRK28-FLAG* expressing line 28-2. Increased expression of *CRK28* did not significantly alter MAPK activation compared to Col-0 after flg22 treatment (Fig 5D). These results suggest that heightened expression of *CRK28* results in an increase of a subset of PTI responses after perception of specific microbial features.

CRK28 associates with BAK1 and is present in the FLS2/BAK1 immune complex

Bacterial flagellin is perceived by the RLK FLS2, whose signaling is dependent on the co-receptor BAK1 (1, 3, 7). Chitin perception in *Arabidopsis* does not require BAK1 (50, 51). Heightened expression of *CRK28* positively affects the flg22-induced ROS burst, but not chitin-induced ROS burst (Fig 5C). Therefore, we sought to examine the role of BAK1 for CRK28-

mediated immune responses. Using co-immunoprecipitation (Co-IP), we examined if BAK1 can associate with CRK28 in *N. benthamiana.* We transiently expressed *35S:CRK28-FLAG* and *35S:BAK1-HA* in *N. benthamiana* and immunoprecipitation was performed with anti-HA agarose beads. Immunoblotting with the anti-FLAG antibody demonstrated that CRK28 can Co-IP with BAK1 in *N. benthamiana* (Fig 6A). To further confirm this association, four-week-old Col-0 and *npro:CRK28-FLAG* line 28-2 were sprayed with 10μM flg22 or water to induce *CRK28* expression and leaves were sampled after 3h. Immunoprecipitation with the anti-BAK1 antibody showed that CRK28-FLAG can Co-IP with BAK1 (Fig 6B).

Fig 6. BAK1 associates with CRK28 in *Arabidopsis* and *Nicotiana benthamiana* and silencing *NbSerk3* reduces CRK28-mediated cell death.

BAK1 forms a ligand-dependent immune complex with multiple PRRs (Pattern recognition receptors) including FLS2 in *Arabidopsis* (1, 7). Recently, Yeh and colleagues have reported that CRK4, CRK6 and CRK36 associate with FLS2 in a flg22 independent manner in *Arabidopsis* protoplasts (22). Thus, we were interested to know whether CRK28 is present in the activated FLS2/BAK1 immune complex. *35S:CRK28-FLAG, 35S:FLS2-GFP* and *35S:BAK1-HA* were transiently expressed in *N. benthamiana*. Twenty-four hours later, leaf tissue was collected 5min after elicitation with 1μM flg22 or water for immunoprecipitations. As expected, the anti-HA immunoblot showed that BAK1 can Co-IP with FLS2 in a ligand dependent manner (Fig 6C) (7). Similar to Yeh and colleagues, we observed that CRK28 can Co-IP with FLS2 in a ligand independent manner (Fig 6C). However, the Co-IP of CRK28, BAK1, and FLS2 was only observed in a flg22 dependent manner (Fig 6C). Although BAK1 typically forms a complex with

primary PRR immune receptors in a ligand dependent manner, some CRK28 can associate with BAK1 in the absence of flg22 treatment (Fig 6A-B). CRK28 is expressed at low levels at a resting state and rapidly induced upon pathogen perception (Fig 2A, 4A, 1D). Under native expression conditions, it is likely that CRK28 association with the FLS2 complex occurs after PTI induced transcription.

Mutating the conserved lysine residue in ATP binding motif (K377N) abrogates CRK28-mediated cell death in *N. benthamiana* (Fig 4A). We investigated the importance of K377 for association with the activated FLS2/BAK1 immune complex. *35S:CRK28^{K377N}-FLAG, 35S:FLS2-GFP* and *35S:BAK1-HA* were transiently expressed in *N. benthamiana*, treated with either water or flg22, and samples were collected 5min later for IP. Similar to wild type CRK28, CRK28^{K377N} can also Co-IP with FLS2-GFP in a flg22 independent manner (Fig 6C). Previous work has also demonstrated for FLS2/BAK1 that kinase activity is not required for immune complex formation (48). These data indicate that kinase activity is not required for CRK28's association with the FLS2/BAK1 immune complex.

CRK28-mediated cell death requires the *AtBAK1* ortholog in *N. benthamiana*

AtBAK1 is a member of the larger somatic embryogenesis-related kinase (*SERK*) family, and the closest *N. benthamiana* homologue of *BAK1* is *NbSerk3* (8). In *N. benthamiana*, *NbSerk3* is required for *NbFLS2* dependent responses and silencing *NbSerk3* significantly affects the flg22-triggered ROS burst (8). We used a virus-induced gene silencing (VIGS) approach to silence *NbSerk3. TRV:GUS* infiltrated plants were used as a negative control. As previously reported,

NbSerk3 silenced plants displayed slight stunting and aberrant leaf morphology (8). Reverse transcriptase PCR (RT-PCR) demonstrated that the transcript level of *NbSerk3* is significantly reduced in *NbSerk3* silenced plants when compared to *TRV:GUS* infiltrated plants (Fig 6E). We transiently expressed *35S:CRK28-FLAG* and *35S:GFP* in *NbSerk3* and *TRV:GUS* infiltrated *N. benthamiana* leaves. Strong cell death was observed when *35S:CRK28-FLAG* was expressed in *TRV:GUS* infiltrated *N. benthamiana* leaves (Fig 6D). *CRK28*-induced cell death was either completely abolished or significantly reduced in all of the *NbSerk3* silenced leaves (Fig 6D). We also confirmed the cell death reduction by trypan blue staining (Fig 6D). As expected, expression of *35S:GFP* did not induce cell death (Fig 6D). Anti-FLAG immunoblotting confirmed that *CRK28* was expressed at similar levels in both *NbSerk3* and *TRV:GUS* infiltrated plants (S7A Fig).

To verify that the reduction of CRK28-induced cell death in *NbSerk3* silenced plants is specific to *CRK28*, we infiltrated *35S:RPS2-FLAG*, an *Arabidopsis* resistance protein known to trigger cell death in *N. benthamiana* (52). *35S:RPS2-FLAG* induces cell death to the same level in both *NbSerk3* and *TRV:GUS* infiltrated leaves (S7B Fig). Anti-FLAG immunoblotting confirmed that *RPS2-FLAG* was expressed at similar levels in both *NbSerk3* silenced and *TRV:GUS* infiltrated leaves (S7C Fig). Overall, these results indicate that *NbSerk3* is required for *CRK28*-induced cell death in *N. benthamiana.* Furthermore, silencing *NbSerk3* specifically affects CRK28-induced cell death but not cell death induced by RPS2.

CRK28 self-associates and associates with CRK29

Multiple studies have demonstrated that receptors assemble into ligand-induced immune complexes to initiate defense signaling (1). Thus, we investigated the ability of CRK28 to self-associate in the presence and absence of immune perception. 35S:CRK28-FLAG and 35S:CRK28-HA were transiently expressed in *N. benthamiana*, 24h later leaf tissue was collected after elicitation with 1μM flg22 or water, and immunoprecipitations were performed with FLAG antibody beads. Anti-HA immunoblotting demonstrated that CRK28-HA can Co-IP with CRK28-FLAG indicating the self-association of CRK28 in *N. benthamiana* (Fig 7A). CRK28 also self-associates after flg22 treatment (Fig 7A).

Fig 7. CRK28 self-associates in *Nicotiana benthamiana* and also associates with CRK29

Next, we examined CRK28's ability to associate with CRK29, a closely related and genetically linked CRK (S3 Fig). 35S:CRK28-HA and CRK29-FLAG were transiently expressed in *N. benthamiana* for 24h. At this point, leaves were collected 5min after elicitation with flg22 or water and immunoprecipitation was performed with anti-FLAG beads. Anti-HA immunoblotting revealed that CRK28-HA can Co-IP with CRK29-FLAG in both flg22 and water treated samples, indicating that CRK28 associates with CRK29 (Fig 7B). Taken together, these results demonstrate that CRK28 self-associates and can also associate with CRK29.

Discussion

Some of the largest gene families in plants encode RLKs with similarity to characterized immune receptors (53). Many of these proteins localize to the plasma membrane and can control pathogen perception as well as propagate signals downstream of pathogen recognition (1, 12).

We reproducibly identified 404 RLKs by MS/MS, revealing a large dynamic range in estimated LRR-RLK abundance (S1 Fig). Most known PRRs are present at relatively low levels in PM fractions (S1 Fig, S2 Fig). PRR abundance is likely tightly controlled in order to avoid inappropriate activation. Pre-treatment of plants with flg22 primes the plant immune system to elicit robust defense responses upon pathogen challenge (3). The up-regulation of many known PRRs (S1 Fig, S2 Fig) around 720min post-flg22 treatment supports a model where the primary recognition event stimulates an increase in pathogen receptors at the plasma membrane, leading to stronger activation of defense responses against subsequent or sustained pathogen attack. The increase in PRRs recognizing different microbial ligands may allow the plant to more rapidly achieve the signaling threshold required for activation of defense. Moreover, the expression patterns of known PRRs strongly implicate uncharacterized RLKs with similar expression profiles as additional plant immune receptors or regulatory proteins.

The tandem duplication of many CRKs on chromosome 4 in *Arabidopsis* is reminiscent of resistance gene clusters in plant genomes and may facilitate adaptive evolution of novel specificity, sub-functionalization, or coordinated gene expression (54). Large scale phenotyping of *CRK* T-DNA insertion lines revealed robust phenotypes related to plant growth and stress adaptation for knockouts in *CRK2* and *CRK5*, respectively (15). However, most individual *CRK* T-DNA insertions exhibited more subtle alterations in plant growth, stomatal responses, and abiotic/biotic responses (15). For example, the *crk28-1* knockdown exhibited a slight increase in visual *Pst* disease symptoms in young plants, which typically exhibit enhanced susceptibility (15, 55). We detected a significant range in CRK protein abundance at a resting state. However, the six CRK proteins that were robustly induced by PTI perception exhibited low-level protein

expression at a resting state (S2 Fig). We hypothesize that the subset of CRKs that exhibited a strong increase in protein abundance after PRR perception and are coordinately involved in immune signaling after initial pathogen perception. Consistent with this hypothesis, inhibiting expression of *CRK22, 28,* and *29* resulted in enhanced susceptibility to *Pst.* Heightened expression of CRK28 in *Arabidopsis* resulted in increased resistance to *Pst* and an increased ROS burst upon flg22 perception. Previous studies have demonstrated that the PEPR1/2 RLKs amplify immune signaling, by perceiving endogenous Pep epitopes whose corresponding *PROPEP* transcripts are rapidly induced upon perception of PAMPs (12, 56, 57). PEPR1 protein abundance also significantly increased after flg22 perception (Fig 1C). Future research is necessary to determine if CRKs act in a similar manner to amplify defense responses.

Pathogen perception induces an extracellular ROS burst (3), and oxidative stress facilitates the formation of multiple intra- and inter-disulfide bonds between cysteine residues (43, 58). Mutating CRK28's cysteine residues predicted to be involved in disulfide bond formation into alanine completely abolished CRK28-mediated cell death in *N. benthamiana,* but did not affect protein stability (Fig 3D-E). Earlier reports have indicated that redox-sensitive cysteine residues and disulfide bonds can serve as a switch to modulate protein function (43, 58). Alterations in apoplastic ROS upon pathogen perception could enhance disulfide bond formation of CRK28 and act as a redox-switch to activate this RLK (15).

Previous studies have demonstrated that post translational modifications (PTMs) play various roles in immune receptor function. We have demonstrated that CRK28 is both glycosylated and phosphorylated *in planta.* Recently, CRK4 was demonstrated to be glycosylated and *STT3a* (*STAUROSPORIN AND TEMPERATURE SENSITIVE3) N*-glycosylation was required for

CRK4-induced cell death and protein accumulation in *Arabidopsis* (39). Glycosylation has also been shown to be important for the function of multiple immune receptors including FLS2, EFR, and Cf proteins (41, 59, 60). Mutation of the *N*-linked glycosylation sites in EFR reduced the level of mature EFR protein, decreased ligand binding, and decreased ligand-elicited ROS burst (41).

RLK-mediated immune signaling is regulated in a phosphorylation dependent manner. For example, FLS2-mediated flg22 perception and signaling requires trans-phosphorylation events that occur in the receptor complex (61). In addition, the transmembrane protein RBOHD, an NADPH oxidase responsible for production of extracellular ROS, is activated through trans-phosphorylation by the receptor-like cytoplasmic kinase BIK1 and calcium dependent protein kinases (62). Mutation of the conserved lysine residue in the kinase domain of the Ser/Thr protein kinases is known to abolish kinase activity and thereby signaling (47, 48). *In vitro* kinase activities have been demonstrated for CRK6, CRK7, and CRK36 (63, 64). The strength of autophosphorylation and co-factor preference varied between different CRKs (63, 64). Although we were unable to detect *in vitro* kinase activity for CRK28, we demonstrated that mutating the lysine residue in the kinase domain of CRK28 abolished its ability to induce cell death in *N. benthamiana* (Fig 4A). Overexpression of *CRK28* in *Arabidopsis* leads to altered developmental phenotypes, but overexpression of $CRK28^{K377N}$ did not (Fig 4D). Furthermore, CRK28 is phosphorylated *in planta.* It is possible that CRK28 is an active kinase, but our purified protein was not properly folded or CRK28 requires additional proteins or co-factors for activity. Alternatively, CRK28 could be transphosphorylated by other plant kinases. Taken together, our

results suggest that an intact kinase domain is required for CRK28-mediated signaling and function.

The BAK1 RLK has been identified as a co-receptor for both primary immune receptors, such as FLS2, as well as signal amplifying RLKs such as PEPR1/2 (1). Here we found that BAK1 is also required for CRK28-mediated cell death induction. Silencing the homolog of *AtBAK1* in *N. benthamiana*, *NbSerk3*, significantly reduced CRK28-induced cell death (Fig 6D). Using immunoprecipitation, we demonstrated BAK1 associates with CRK28. Consistent with the requirement of BAK1 for CRK28 induced cell death, increased expression of CRK28 resulted in a higher flg22-triggered ROS burst, but did not affect chitin-triggered ROS burst (Fig 5B-C). While FLS2 perception of flg22 requires BAK1, perception of chitin occurs in a BAK1 independent manner (50, 51). BAK1 often associates with immune receptors in a ligand dependent manner (1). Although the ligand for CRKs is still unknown, BAK1/CRK28 association does not depend on flg22. CRK28 interacted with FLS2 in flg22 independent manner. In addition, we identified CRK28 in the FLS2/BAK1 immune complex. CRK28's expression is very weak at a resting state. Thus, during natural infection, substantial CRK28 protein synthesis would likely first require initial pathogen perception mediated by other PRRs such as FLS2. Future research focusing on the role of additional suites of CRKs for enhancing plant defense responses as well as elucidating the ligand(s) perceived by these RLKs could facilitate targeted engineering for increased disease resistance.

Materials and Methods

Plant materials and growth conditions

A. thaliana plants were grown in a controlled environment chamber at 23˚C, 75% relative humidity, and a 10h/14h light/dark photoperiod with light intensity of 100μE.m^{-2}·S^{-1}. All seeds were stratified for 3-4 days at 4ºC before sowing into soil. *Nicotiana benthamiana* plants were grown in a controlled environmental chamber at 25°C, 85% relative humidity, 16/8-hr light/dark photoperiod with light intensity of 180μE.m^{-2}· S^{-1}.

For the plasma membrane (PM) proteome experiments, four to five week-old plants were used. Three hours after the onset of light, Col-0 plants were sprayed with 10μM flg22 peptide (>91.6% purity, GenScript USA Inc.) in 18.2 MΩ·cm^{-1} water containing 0.025% Silwet L-77 surfactant using a Preval-267 compressed air sprayer. Col-0 plants sprayed with 18.2 MΩ·cm^{-1} water containing 0.025% Silwet L-77 were used as a negative control. Plants were incubated for the indicated time period before harvesting tissue for protein isolations. Three biological replicates of plants grown and harvested at different times were performed. Water- and flg22- treated samples were processed in parallel for all replications.

T-DNA insertion lines in *CRK28* (*crk28-1*, SALK_085178), and *CRK29* (*crk29-1*, SALK_069665) in the Col-0 background were obtained from the Arabidopsis Biological Resource Center (ABRC), and the lines were genotyped by PCR to identify homozygous insertion lines and transcript expression was analyzed by RT-PCR. Primers used in all experiments are shown in S2 Table.

Plasma membrane enrichment and processing

PM enrichment was performed on 30-40g of leaf tissue using three rounds of aqueous two-phase partitioning as described previously (65)with minor modifications. Homogenization buffer was supplemented with 50mM sodium pyrophosphate, 25mM sodium fluoride, 1mM sodium molybdate, 1mM Sodium orthovanadate, and 25mM β-glycerophosphate. The final upper phase fraction containing enriched plasma membrane vesicles was incubated with 0.02% Brij-58 detergent on ice for 10min to invert vesicles and release cytosolic proteins (66). Samples were diluted 20 times with water and centrifuged at 90000g for 60min to pellet plasma membrane vesicles. Membrane pellets were frozen in liquid nitrogen and stored at -80˚C. Protein samples were solubilized in 2X Laemmli buffer with 6M urea and quantified using the RCDC Protein Assay (Biorad). Samples (300µg protein) were fractionated by 1D SDS-PAGE using an 8-16% Precise Protein Gradient Gel (Thermo Scientific). The entire sample lane was excised and cut into 15 pieces of equal size using a disposable grid cutter (The Gel Company). In-gel digestions were performed with trypsin (67). Digested peptides were dried using a vacuum concentrator then solubilized in 60µL 2% acetonitrile/0.1% trifluoroacetic acid and frozen at -80C.

LC-MS/MS

The LC-MS/MS system configuration consisted of a CTC Pal autosampler (LEAP Technologies) and Paradigm HPLC (Michrom BioResources) coupled to a QExactive hybrid quadrupole Orbitrap mass spectrometer (Thermo Scientific) with a CaptiveSpray ionization source (Michrom BioResources). LC was performed by injecting 20µL of each peptide sample onto a Zorbax300SB-C18 trap column (5µm, 5x0.3mm, Agilent Technologies) and desalted online. Peptides were eluted from the trap and separated on a reverse-phase Michrom Magic C18AQ (200µm x 150mm) capillary column at a flow rate of 2 µL/min using a 120min gradient (2 to

35% buffer B 85min, 35 to 80% buffer B 25min, 2% buffer B 10min; buffer A=0.01% formic acid in H2O, buffer B=100% acetonitrile). The mass spectrometer was operated in data-dependent acquisition mode using a standard Top15 method. The 30 protein fractions for each biological replicate were analyzed on the same column in blocks of seven and eight, alternating between flg22- and water-treated samples separated with multiple column flushes.

Protein identifications

Tandem mass spectra were extracted to mzML format using Proteome Discoverer and analyzed with the X!Tandem GPM-XE Cyclone version 2013.02.01.2 spectrum modeler (68) using the TAIR10 *Arabidopsis* complete proteome (TAIR10_pep_20101214.fasta, 35386 entries) with a list of common contaminants (112 entries). A reversed and concatenated database served as a decoy sequence database to determine peptide and protein false discovery rates (FDR) (69). X!Tandem was configured to allow parent ion mass error of 20ppm and fragment mass error of 20ppm. Data were searched using fixed modification of +57 (carbamidomethyl) modification of cysteine residues and the following variable modifications: -18 on N-term E (Glu->pyro-Glu), -17 on N-term (Ammonia-loss), -17 on N-term Q (Gln->pyro-Glu), +1 on NQ (Deamidated), +16 on MW (Oxidation), +32 on MW (Dioxidation), +42 on Kn (Acetyl), +80 on STY (Phospho) while allowing one missed cleavage. X!Tandem search results were imported into Scaffold 4.0.3 (Proteome Software) with all MS/MS runs corresponding to the same sample merged. The probability of peptide identifications was modeled using a local FDR algorithm and discriminant scoring with a naïve Bayes classifier within Scaffold. Protein identifications required two unique peptides, 90.0% protein probability, and 90.0% peptide probability resulting in a 0.1% peptide decoy FDR and 3.1% protein decoy FDR. Shared spectral count distributions was performed

within Scaffold similar to (70) using each protein's cumulative unique peptide identification probability as the distribution factor. Spectral counts of protein isoforms mapping to the same genomic locus were summed. Proteins with more than one spectral count in two of three biological replicates were used for differential expression analysis. Raw MS/MS data was uploaded to the MassIVE repository (Accession MSV000079639, data will be released upon publication).

Protein Quantitative Analysis

The intersection of two statistical frameworks (QPROT and edgeR) was used to generate a list of high-confidence proteins exhibiting differential abundance (24, 25). In QPROT v1.3.3, spectral counts were modeled as observations from a Poisson distribution using an empirical Bayes FDR estimation procedure using normalization and accounting for batch effects between biological replicates (24). In edgeR v3.8.6, spectral counts are modeled from a negative binomial distribution using a generalized linear model with replicate and treatment as model factors (25). For both QPROT and edgeR, proteins with an FDR ≤ 0.05 and an estimated $|\text{Log}_2$ fold change$| > 0.58$ (50%) were classified as differentially expressed (S1 Table).

Phylogenetic analyses

Clustal X 2.1 (71) was used to align RLK kinase domain sequences (26) using the neighbor-joining method under default settings. Aminoglycoside 3'-phosphotransferase (P0A3Y6) was used as the outgroup for the kinase domain phylogenies (26). To construct the phylogenetic tree of CRKs located on chromosome 4, the full-length amino acid sequences were downloaded from TAIR10. The protein sequences were aligned using Clustalw2

(http://www.ebi.ac.uk/Tools/msa/clustalw2/) and a phylogenetic tree was generated using the neighbour-joining method and the tree was visualized using FigTree v1.4.2 (http://tree.bio.ed.ac.uk/software/figtree/).

Molecular cloning

To generate a native promoter *CRK28* expression construct, the 745bp upstream of *CRK28's* start codon was amplified along with the genomic DNA of *CRK28* with CRK28_promoter_F and CRK28_Rev primer pair. The resulting PCR fragment was cloned into pENTR/D-TOPO vector (Invitrogen) and moved into the binary vector pGWB1-3xFLAG using gateway technology (Invitrogen) generating *npro:CRK28-3xFLAG*. The binary vector pGWB1-3xFLAG was modified from pGWB1 to contain C-terminal 3xFLAG. To modify pGWB1, the gateway cassette (GW) with 3xFLAG tag was amplified from a gateway compatible binary vector pTA700-3xFLAG with a forward and reverse primer pair containing *Hind*III and *Sac*I restriction sites, respectively. Then the GW cassette from pGWB1 was removed by *Hind*III/*Sac*I digestion and replaced with the PCR product containing GW-3xFLAG generating pGWB1-3xFLAG.

To generate a *CRK28* over-expression construct driven by the CaMV 35S promoter, the *CRK28* cDNA was amplified with the CRK28_F and CRK28_R primer pair. The PCR fragment was then cloned into pENTR/D-TOPO vector. The ATP-binding site (K377) in kinase domain of CRK28 and the extracellular cysteine residues (C99, C127, C214, C242) were mutated into asparagine and alanine by site directed mutagenesis in pENTR/D-TOPO vector (Stratagene), respectively. All the constructs were moved into the gateway compatible binary vector pMD1-3xFLAG to generate 35S:CRK28-3xFLAG, 35S:CRK28^{K377N}-3xFLAG, 35S:CRK28^{C99A}-

3xFLAG, 35S:CRK28^{C127A}-3xFLAG, 35S:CRK28^{C214A}-3xFLAG, and 35S:CRK28^{C242A}-3xFLAG.

Plant transformation

The *npro:CRK28-3xFLAG* was transformed into the *crk28-1* mutant. *35S:CRK28-3xFLAG* and *35S:CRK28^{K377N}-3xFLAG* were transformed into Col-0. All the constructs were transformed into *Arabidopsis* following the floral dip protocol with *Agrobacterium tumefaciens* strain GV3101 (72).

Reverse transcriptase PCR (RT-PCR) and Quantitative real-time PCR (qPCR)

To confirm *crk28-1*, and *crk29-1* were true knockouts by RT-PCR, the mutants and Col-0 rosette leaves were infiltrated with 1µM flg22 and 3h later, the leaves were sampled in liquid nitrogen. Total RNA was extracted from rosette leaves following a Trizol based RNA extraction protocol. One µg of RNA, in a total reaction volume of 20µl, was used to synthesize cDNA using M-MLV reverse transcriptase (Promega). Specific primer pairs for each T-DNA insertion line or target genes of VIGS were used for RT-PCR and the PCR was run for 25 cycles or for indicated number of cycles. In the case of qPCR, the CFX96 real-time PCR detection system (Bio-Rad) was used to quantify expression of the genes. The *Arabidopsis Actin 2 (ACT2), Ubiquitin 1 (UBQ1)* and *Elongation Factor One alpha* (*EF-1a)* genes were used as endogenous controls in RT-PCR and qPCR, respectively. In *N. benthamiana*, the *NbEF-1a* gene was used as an endogenous control. All the primers used in qPCR and RT-PCR in this study are presented in Table S1.

688 **Pathogen assays**

689 Four-week-old *Arabidopsis* plants grown as described above were used for pathogen assays. *P.*
690 *syringae* pv. *tomato* (*Pst*) strain DC3000 and *Pst* DC3000 Δ*hrcC*, were used for plant
691 inoculations. Strains were grown on plates containing 100µg/mL Rifampicin and 25µg/mL
692 Kanamycin overnight at 28°C. Inoculum was prepared in 5mM and 10mM $MgCl_2$ for infiltration
693 ($3x10^5$ CFU/mL) and spray inoculation ($1x10^9$ CFU/mL), respectively. For flg22 protection
694 assays, leaves were infiltrated with 1µM flg22 and 24hrs later the same leaves were infiltrated
695 with *Pst* DC3000. After inoculation, the plants were covered for 24hrs to maintain high humidity
696 and symptoms were monitored overtime. Four days post-inoculation, six leaves were sampled
697 from four plants and surface sterilized with 70% ethanol for 30s. Bacterial titers were determined
698 as previously described (73).

699

700 **ROS burst assay**

701 Leaf discs were collected using cork border (5mm diameter) from three-week-old *Arabidopsis*
702 plants and floated overnight in demineralized water. The next day, the water was replaced with
703 an assay solution containing 17mg/ml luminol (Sigma), 10mg/ml horse radish peroxidase
704 (Sigma), 100nM flg22 (Genscript), or 50µg/ml chitin (Sigma). Luminescence was measured
705 using Tristar multimode reader (Berthold technology). Statistical differences were calculated
706 with Fisher's LSD, alpha 0.05. At least 24 leaf discs were used in each replication and the
707 experiment was repeated more than three times with similar results.

708

709 **MAPK assay**

Four-week-old Col-0 and the CRK28 expressing line (28-2) were sprayed with 10μM flg22 or water (control) with 0.025% Silwett L-77. Leaf samples were collected at 0 (before spray), 5, 15, 30 and 45 minutes time points. Samples were ground in liquid nitrogen and re-suspended in 200μl extraction buffer (50 mM HEPES (pH 7.5), 50 mM NaCl, 10 mM EDTA, 0.2% Triton X-100, 1X protease inhibitor cocktail (Sigma), and 1X Halt phosphatase inhibitor cocktail (Thermo scientific). After centrifugation for 10 minutes at 10K RPM, the supernatants were transferred into new tubes and the total protein concentration was quantified using pierce 660nm protein assay (Thermo scientific) following the manufacturer's protocol. Equal amount of protein samples were separated on 12% SDS PAGE and immunoblotted with anti-p44/42 MAPK antibody (Cell Signaling Technology).

Virus Induced Gene Silencing in *Arabidopsis*

The DNA fragments of *CRK28* and *CRK22* (~400 bp of each starting from ATG start codon) were amplified from Col-0 cDNA. *CRK28* was digested with *Eco*RI and *Kpn*I and cloned into pTRV-RNA2 (pYL156) yielding pYL156-CRK28. The *CRK22* fragment was digested with *Nco*I and *Kpn*I and cloned into pYL156-CRK28 via the same restriction sites. The construct pYL156-CRK28/22 contains two fragments targeting *CRK28* and *CRK22*, respectively. The binary TRV vectors, pTRV-RNA1, pYL156-GFP, pYL156-Cla1, and pYL156-CRK28/22 were electroporated into *Agrobacterium tumefaciens* strain GV3101 and VIGS was performed as previously described on two-week-old plants (39). The pYL156-Cla1 silenced plants exhibit a leaf bleaching phenotype, which was used as a visual marker for silencing efficiency (39). One pair of fully expanded leaves on the four-week-old plants were inoculated with *Pst* DC3000 and bacterial titers were determined 3dpi.

733

734 The leaves of four-week-old VIGSed plants were treated with 100nM flg22 for 1 h (or H2O as
735 control) in order to induce *CRK* expression. TRIzol reagents (Invitrogen) were used for RNA
736 extraction. After DNAase I treatment (37°C x 30min), the RNAs were reverse-transcribed into
737 cDNA by using MLV reverse transcriptase (New England Biolabs). RT-PCR with the primers
738 listed in Table S2 was used to detect target transcript levels after VIGS. For CRK genes, 30 PCR
739 cycles (98C°, 10s, 58°C, 15s, 72°C 30s) were used. For UBQ1, 22 PCR cycles were performed.

740

741 **Immunoprecipitation (IP)**

742 For IP in *N. benthamiana,* constructs cloned into binary vectors (35S:CRK28-3xFLAG,,
743 35S:BAK1-3xHA, 35S:CBL-GFP-3xFLAG/35S:GFP, 35S:CRK29-3xFLAG, and 35S:FLS2-
744 GFP) were transformed into *A. tumefaciens* strain C58C1 and infiltrated into leaves at
745 concentration of $2x10^8$CFU/mL for 35S:CRK28-3xFLAG and 35S:BAK1-3xHA and
746 $6x10^8$CFU/mL for 35S:FLS2-GFP. One gram of leaf tissue was collected at 24hpi and frozen in
747 liquid nitrogen. In the case of induction by elicitor, 1µM flg22 or water was infiltrated into
748 leaves just before the leaves start visually showing cell death (~20-22hpi with the constructs) and
749 samples were collected 5 minutes later.

750

751 To perform IPs in *N. benthamiana* tissue, the samples were ground by mortar and pestle in liquid
752 nitrogen and homogenized in IP buffer (50mM Tris pH7.4, 150mM NaCl, 0.5% Triton X-100,
753 6mM 2-Mercaptoethanol and 1x complete protease inhibitor). The homogenate was pre-cleared
754 by centrifugation at 14K RPM for 20 minutes and further filtered using two layers of cheesecloth.
755 Thirty µl of anti-FLAG (Sigma) and anti-HA (Thermo Fisher Scientific), and 25µl of anti-GFP

(Chromotek) agarose beads were used for each sample. Beads were washed twice with IP buffer, added to the homogenate, and incubated at 4°C rotating end-to-end for 4hrs. Beads were pelleted by centrifugation at 3K RPM for 3 minutes, washed 3 times with 1ml IP buffer without 2-mercaptoethanol and re-suspended in 3x laemmli buffer. After boiling for 5 min, the protein samples were separated by SDS-PAGE and subsequently immunoblotted with the respective antibodies. The concentrations of antibodies used in this study were as follows: anti-FLAG HRP (Sigma, 1:3000), anti-GFP HRP (Miltenyi Biotec, 1:3,000), anti-HA HRP (Roche, 1:2,000), and anti-BAK1 (Agrisera, 1:5000).

In Arabidopsis, four-week-old plants were sprayed with 10µM flg22 or water containing 0.025% Silwet L-77. Three hour later, 1 gram of leaf tissues were collected in liquid nitrogen. Sample processing and IP was performed as described for *N. benthamiana*.

Self-association assays

In order to assay CRK28 self-association, 35S:CRK28-3xFLAG and 35S:CRK28-3xHA were co-expressed in *N. benthamiana* leaves. 35S:CRK28-3xFLAG and 35S:CRK28-3xHA were also individually expressed in *N. benthamiana* at the same time. In addition, 35S:CRK28-3xHA was co-expressed with 35S:CRK29-3xFLAG to investigate if CRK28 also heterodimerizes with CRK29. Before sampling for IP, the leaves were infiltrated with 1µM flg22 or water and one gram leaf tissue was collected 5 minutes after treatment. Sample processing and IP were performed as described above.

Purification of CRK28's kinase domain from *E. coli*

779 The kinase domain of CRK28 and its kinase dead variant (K377N) (amino acids: 349-623) were
780 cloned into the *E. coli* expression vector pMAL-C4x (49) with an N-terminal fusion to MBP.
781 Briefly, the kinase domain of *CRK28* and its kinase dead variant were PCR amplified with the
782 KD*BamH*I-F and KD*Pst*I_R primer pairs containing *BamH*I and *Pst*I restriction sites,
783 respectively. The PCR products were digested and cloned into pMAL-C4x using *BamH*I and *Pst*I
784 restriction enzymes.
785
786 For protein expression and purification, the constructs were transformed into the *E. coli* strain
787 Rosette DE3. A 500ml culture was grown at 37ºC until the cell density reached OD_{600} = 0.5. The
788 culture was then transferred to a 16ºC incubator for 1hr, and then 0.3mM IPTG was added to
789 induce protein expression for 7h. The *E. coli* culture was harvested by centrifugation at 12K
790 RPM for 10minutes. The pellet was then re-suspended in column buffer (20 mM Tris-HCl, 200
791 mM NaCl, 1mM EDTA, 1mM PMSF, 10µM Leupeptin and 10µg/ml lysozyme) and the proteins
792 were purified using amylose resin (New England Biolabs). RIPK was purified as previously
793 described (49).
794
795 **Kinase activity assay**
796 To perform an *in vitro* kinase activity assay with recombinant proteins, three µg of CRK28,
797 $CRK28^{K377N}$, and RIPK (*AT2G05940*, positive control) proteins were mixed with 100µM ATP
798 and 3µg of the kinase substrate myelin basic protein (MyBP) in a kinase buffer (50mM Hepes
799 pH7.5, 10mM $MgCl_2$, 50mM NaCl, and 1mM DTT) and incubated at 30ºC for 1hr. The reactions
800 were stopped by adding 3xlaemmli buffer, boiled for 5 minutes, and separated on 10% SDS
801 PAGE. The proteins were transferred onto PVDF membrane (Millipore), blocked by 5% BSA

for 1hr at room temperature and incubated overnight 4ºC with anti-phospho-threonine antibody in 5% BSA. Membranes were developed using chemiDoc Touch imaging system (Bio Rad). A radioactive kinase activity assay was also performed by adding 10 µCi of (32P)-γ-ATP (Perkin Elmer) and incubating at 37ºC for 1h. The reaction was stopped by adding 5x laemmli buffer, incubated at 60ºC for 5 minutes, and run on a 12% Precise Tris-Hepes SDS-PAGE (Thermo Scientific) and visualized by autoradiography.

To assess kinase activity and phosphorylation *in planta*, 35S:CRK28-3xFLAG and 35S:CRK28^{K377N}-3xFLAG were transiently expressed in *N. benthamiana* and at 24hpi, 2g of infiltrated leaves were collected in liquid nitrogen. The samples were ground in 3ml IP buffer and an IP was performed with anti-FLAG conjugated agarose bead as described above. After the third wash with IP buffer, the beads were washed once with kinase buffer (50mM Hepes pH7.5, 10mM $MgCl_2$, 10mM $MnCl_2$, 0.1mM $CaCl_2$, 1mM DTT) and finally the beads were re-suspended in 50µl kinase buffer. Twenty µl of the re-suspended beads were used in kinase assay as described above for the *in vitro* kinase assays.

Virus-Induced Gene Silencing (VIGS) of *NbSerk3*

All the VIGS constructs targeting *NbSerk3* (pTRV2-NbSerk3), *GUS* (pTRV2-GUS), and *Phytoene desaturase* (*PDS)* (pTRV2-PDS) including the pTRV1 were obtained from Gregory B Martin (74). Bacterial growth cultures and preparation for infiltration were performed as previously described (75) with slight modification. Briefly, an overnight *Agrobacterium* cultures (strain GV3101) at OD_{600} = 2 carrying pTRV2-NbSerk3, pTRV2-GUS and pTRV2-PDS were mixed with GV3101 carrying pTRV1 (OD_{600} = 2) in 1:1 ratio and infiltrated into cotyledons of

ten-day-old *N. benthamiana* seedlings. Three weeks later, *Agrobacterium* cultures carrying *35S:CRK28-3xFLAG* (OD_{600} = 0.3)*, 35S:RPS2-3xFLAG* (OD_{600} = 0.3)*,* and *35S:CBL-GFP-3xFLAG* (OD_{600} = 0.3) were infiltrated into *NbSerk3* and *TRV:GUS* infiltrated *N. benthamiana* plants and cell death was monitored over time.

Enzymatic deglycosylation assay

To enzymatically deglycosylate CRK28, 35S:CRK28-3xFLAG was transiently expressed in *N. benthamiana*. Twenty-five hpi, 0.5gram of infiltrated leaves were collected in liquid nitrogen. Sample processing and the PNGase F and EndoHf enzymatic deglycosylation assays were performed as described in (40). Ten µl of the reaction was separated on a 10% SDS PAGE and immunoblotted with the anti-FLAG antibody (Sigma, 1:3,000). To investigate if there CRK28 carries the *N*-linked glycan complexes, 35S:CRK28-3xFLAG, 35S:CRK28^{K377N}-3xFLAG and 35S:GFP were transiently expressed in *N. benthamiana*. IP was performed with anti-FLAG antibody and immunoblotted with anti-HRP (Jackson ImmunoResearch) as previously described (59).

Acknowledgements

We thank Tania Y. Toruño**,** Thomas WH. Liebrand, and DongHyuk Lee for their comments on the manuscript.

References

1. Zipfel C. Plant pattern-recognition receptors. Trends in Immunology. 2014;35(7):345-51.
2. Chiang Y-H, Coaker G. Effector Triggered Immunity: NLR Immune Perception and Downstream Defense Responses. The Arabidopsis Book. 2015;13: e0183. 2015
3. Boller T, Felix G. A Renaissance of Elicitors: Perception of Microbe-Associated Molecular Patterns and Danger Signals by Pattern-Recognition Receptors. Annual Review of Plant Biology. 2009;60(1):379-406.
4. Dou D, Zhou J-M. Phytopathogen Effectors Subverting Host Immunity: Different Foes, Similar Battleground. Cell Host & Microbe. 2012;12(4):484-95.
5. Sánchez-Vallet A, Saleem-Batcha R, Kombrink A, Hansen G, Valkenburg D-J, Thomma BP, et al. Fungal effector Ecp6 outcompetes host immune receptor for chitin binding through intrachain LysM dimerization. eLife. 2013;2013;2:e00790.
6. Chinchilla D, Bauer Z, Regenass M, Boller T, Felix G. The Arabidopsis Receptor Kinase FLS2 Binds flg22 and Determines the Specificity of Flagellin Perception. The Plant Cell. 2006;18(2):465-76.
7. Chinchilla D, Zipfel C, Robatzek S, Kemmerling B, Nurnberger T, Jones JDG, et al. A flagellin-induced complex of the receptor FLS2 and BAK1 initiates plant defence. Nature. 2007;448(7152):497-500.
8. Heese A, Hann DR, Gimenez-Ibanez S, Jones AME, He K, Li J, et al. The receptor-like kinase SERK3/BAK1 is a central regulator of innate immunity in plants. Proceedings of the National Academy of Sciences. 2007;104(29):12217-22.
9. Roux M, Schwessinger B, Albrecht C, Chinchilla D, Jones A, Holton N, et al. The Arabidopsis Leucine-Rich Repeat Receptor–Like Kinases BAK1/SERK3 and BKK1/SERK4 Are Required for Innate Immunity to Hemibiotrophic and Biotrophic Pathogens. The Plant Cell. 2011;23(6):2440-55.
10. Liebrand TWH, van den Burg HA, Joosten MHAJ. Two for all: receptor-associated kinases SOBIR1 and BAK1. Trends in Plant Science. 2014;19(2):123-32.
11. Osakabe Y, Yamaguchi-Shinozaki K, Shinozaki K, Tran L-SP. Sensing the environment: key roles of membrane-localized kinases in plant perception and response to abiotic stress. Journal of Experimental Botany. 2013;64(2):445-58.
12. Huffaker A, Ryan CA. Endogenous peptide defense signals in Arabidopsis differentially amplify signaling for the innate immune response. Proceedings of the National Academy of Sciences. 2007;104(25):10732-6.
13. Chen Z. A Superfamily of Proteins with Novel Cysteine-Rich Repeats. Plant Physiology. 2001;126(2):473-6.
14. Ohtake Y, Takahashi T, Komeda Y. Salicylic Acid Induces the Expression of a Number of Receptor-Like Kinase Genes in Arabidopsis thaliana. Plant and Cell Physiology. 2000;41(9):1038-44.
15. Bourdais G, Burdiak P, Gauthier A, Nitsch L, Salojärvi J, Rayapuram C, et al. Large-Scale Phenomics Identifies Primary and Fine-Tuning Roles for CRKs in Responses Related to Oxidative Stress. PLoS Genet. 2015;11(7):e1005373.
16. Amari K, Boutant E, Hofmann C, Schmitt-Keichinger C, Fernandez-Calvino L, Didier P, et al. A Family of Plasmodesmal Proteins with Receptor-Like Properties for Plant Viral Movement Proteins. PLoS Pathog. 2010;6(9):e1001119.
17. Lee J-Y, Wang X, Cui W, Sager R, Modla S, Czymmek K, et al. A Plasmodesmata-Localized Protein Mediates Crosstalk between Cell-to-Cell Communication and Innate Immunity in Arabidopsis. The Plant Cell. 2011;23(9):3353-73.
18. Caillaud M-C, Wirthmueller L, Sklenar J, Findlay K, Piquerez SJM, Jones AME, et al. The Plasmodesmal Protein PDLP1 Localises to Haustoria-Associated Membranes during Downy Mildew Infection and Regulates Callose Deposition. PLoS Pathog. 2014;10(11):e1004496.
19. Chen K, Du L, Chen Z. Sensitization of defense responses and activation of programmed cell death by a pathogen-induced receptor-like protein kinase in Arabidopsis. Plant Mol Biol. 2003;53(1-2):61-74.
20. Chen K, Fan B, Du L, Chen Z. Activation of hypersensitive cell death by pathogen-induced receptor-like protein kinases from Arabidopsis. Plant Mol Biol. 2004;56(2):271-83.
21. Wrzaczek M, Brosche M, Salojarvi J, Kangasjarvi S, Idanheimo N, Mersmann S, et al. Transcriptional regulation of the CRK/DUF26 group of Receptor-like protein kinases by ozone and plant hormones in Arabidopsis. BMC Plant Biology. 2010;10(1):95.

22. Yeh Y-H, Chang Y-H, Huang P-Y, Huang J-B, Zimmerli L. Enhanced Arabidopsis pattern-triggered immunity by overexpression of cysteine-rich receptor-like kinases. Frontiers in Plant Science. 2015;6:322.
23. Acharya BR, Raina S, Maqbool SB, Jagadeeswaran G, Mosher SL, Appel HM, et al. Overexpression of CRK13, an Arabidopsis cysteine-rich receptor-like kinase, results in enhanced resistance to Pseudomonas syringae. The Plant Journal. 2007;50(3):488-99.
24. Choi H, Kim S, Fermin D, Tsou C-C, Nesvizhskii AI. QPROT: Statistical method for testing differential expression using protein-level intensity data in label-free quantitative proteomics. Journal of Proteomics. 2015;129:121-6.
25. Robinson MD, McCarthy DJ, Smyth GK. edgeR: a Bioconductor package for differential expression analysis of digital gene expression data. Bioinformatics. 2010;26(1):139-40.
26. Shiu S-H, Karlowski WM, Pan R, Tzeng Y-H, Mayer KFX, Li W-H. Comparative Analysis of the Receptor-Like Kinase Family in Arabidopsis and Rice. The Plant Cell. 2004;16(5):1220-34.
27. DeYoung BJ, Bickle KL, Schrage KJ, Muskett P, Patel K, Clark SE. The CLAVATA1-related BAM1, BAM2 and BAM3 receptor kinase-like proteins are required for meristem function in Arabidopsis. The Plant Journal. 2006;45(1):1-16.
28. Stenvik G-E, Tandstad NM, Guo Y, Shi C-L, Kristiansen W, Holmgren A, et al. The EPIP Peptide of INFLORESCENCE DEFICIENT IN ABSCISSION Is Sufficient to Induce Abscission in Arabidopsis through the Receptor-Like Kinases HAESA and HAESA-LIKE2. The Plant Cell. 2008;20(7):1805-17.
29. Tabata R, Sumida K, Yoshii T, Ohyama K, Shinohara H, Matsubayashi Y. Perception of root-derived peptides by shoot LRR-RKs mediates systemic N-demand signaling. Science. 2014;346(6207):343-6.
30. Zipfel C, Kunze G, Chinchilla D, Caniard A, Jones JDG, Boller T, et al. Perception of the Bacterial PAMP EF-Tu by the Receptor EFR Restricts Agrobacterium-Mediated Transformation. Cell. 2006;125(4):749-60.
31. Beck M, Zhou J, Faulkner C, MacLean D, Robatzek S. Spatio-Temporal Cellular Dynamics of the Arabidopsis Flagellin Receptor Reveal Activation Status-Dependent Endosomal Sorting. The Plant Cell. 2012;24(10):4205-19.
32. Lu D, Lin W, Gao X, Wu S, Cheng C, Avila J, et al. Direct Ubiquitination of Pattern Recognition Receptor FLS2 Attenuates Plant Innate Immunity. Science. 2011;332(6036):1439-42.
33. Smith JM, Salamango DJ, Leslie ME, Collins CA, Heese A. Sensitivity to Flg22 Is Modulated by Ligand-Induced Degradation and de Novo Synthesis of the Endogenous Flagellin-Receptor FLAGELLIN-SENSING2. Plant Physiology. 2014;164(1):440-54.
34. Cao Y, Liang Y, Tanaka K, Nguyen CT, Jedrzejczak RP, Joachimiak A, et al. The kinase LYK5 is a major chitin receptor in Arabidopsis and forms a chitin-induced complex with related kinase CERK1. eLife. 2014;2014;3:e03766.
35. Ranf S, Gisch N, Schaffer M, Illig T, Westphal L, Knirel YA, et al. A lectin S-domain receptor kinase mediates lipopolysaccharide sensing in Arabidopsis thaliana. Nat Immunol. 2015;16(4):426-33.
36. Brutus A, Sicilia F, Macone A, Cervone F, De Lorenzo G. A domain swap approach reveals a role of the plant wall-associated kinase 1 (WAK1) as a receptor of oligogalacturonides. Proceedings of the National Academy of Sciences. 2010;107(20):9452-7.
37. Kunze G, Zipfel C, Robatzek S, Niehaus K, Boller T, Felix G. The N Terminus of Bacterial Elongation Factor Tu Elicits Innate Immunity in Arabidopsis Plants. The Plant Cell. 2004;16(12):3496-507.
38. Zipfel C, Robatzek S, Navarro L, Oakeley EJ, Jones JDG, Felix G, et al. Bacterial disease resistance in Arabidopsis through flagellin perception. Nature. 2004;428(6984):764-7.
39. de Oliveira MVV, Xu G, Li B, de Souza Vespoli L, Meng X, Chen X, et al. Specific control of Arabidopsis BAK1/SERK4-regulated cell death by protein glycosylation. Nature Plants. 2016;2:15218.
40. Peter C, Repetti PP, Day B, Dahlbeck D, Mehlert A, Staskawicz BJ. Overexpression of the plasma membrane-localized NDR1 protein results in enhanced bacterial disease resistance in Arabidopsis thaliana. The Plant Journal. 2004;40(2):225-37.
41. Häweker H, Rips S, Koiwa H, Salomon S, Saijo Y, Chinchilla D, et al. Pattern Recognition Receptors Require N-Glycosylation to Mediate Plant Immunity. Journal of Biological Chemistry. 2010;285(7):4629-36.
42. Henquet M, Lehle L, Schreuder M, Rouwendal G, Molthoff J, Helsper J, et al. Identification of the Gene Encoding the α1,3-Mannosyltransferase (ALG3) in Arabidopsis and Characterization of Downstream N-Glycan Processing. The Plant Cell. 2008;20(6):1652-64.
43. Feige MJ, Hendershot LM. Disulfide bonds in ER protein folding and homeostasis. Current Opinion in Cell Biology. 2011;23(2):167-75.
44. Wedemeyer WJ, Welker E, Narayan M, Scheraga HA. Disulfide Bonds and Protein Folding†. Biochemistry. 2000;39(15):4207-16.

45. Waszczak C, Akter S, Jacques S, Huang J, Messens J, Van Breusegem F. Oxidative post-translational modifications of cysteine residues in plant signal transduction. Journal of Experimental Botany. 2015;66(10):2923-34.
46. Hanks S, Quinn A, Hunter T. The protein kinase family: conserved features and deduced phylogeny of the catalytic domains. Science. 1988;241(4861):42-52.
47. Lin Z-JD, Liebrand TWH, Yadeta KA, Coaker G. PBL13 Is a Serine/Threonine Protein Kinase That Negatively Regulates Arabidopsis Immune Responses. Plant Physiology. 2015;169(4):2950-62.
48. Schulze B, Mentzel T, Jehle AK, Mueller K, Beeler S, Boller T, et al. Rapid Heteromerization and Phosphorylation of Ligand-activated Plant Transmembrane Receptors and Their Associated Kinase BAK1. Journal of Biological Chemistry. 2010;285(13):9444-51.
49. Liu J, Elmore JM, Lin Z-JD, Coaker G. A Receptor-like Cytoplasmic Kinase Phosphorylates the Host Target RIN4, Leading to the Activation of a Plant Innate Immune Receptor. Cell Host & Microbe. 2011;9(2):137-46.
50. Gimenez-Ibanez S, Hann DR, Ntoukakis V, Petutschnig E, Lipka V, Rathjen JP. AvrPtoB Targets the LysM Receptor Kinase CERK1 to Promote Bacterial Virulence on Plants. Current Biology. 2009;19(5):423-9.
51. Shan L, He P, Li J, Heese A, Peck SC, Nürnberger T, et al. Bacterial Effectors Target the Common Signaling Partner BAK1 to Disrupt Multiple MAMP Receptor-Signaling Complexes and Impede Plant Immunity. Cell Host & Microbe. 2008;4(1):17-27.
52. Day B, Dahlbeck D, Huang J, Chisholm ST, Li D, Staskawicz BJ. Molecular Basis for the RIN4 Negative Regulation of RPS2 Disease Resistance. The Plant Cell. 2005;17(4):1292-305.
53. Shiu S-H, Bleecker AB. Expansion of the Receptor-Like Kinase/Pelle Gene Family and Receptor-Like Proteins in Arabidopsis. Plant Physiology. 2003;132(2):530-43.
54. Bergelson J, Kreitman M, Stahl EA, Tian D. Evolutionary Dynamics of Plant R-Genes. Science. 2001;292(5525):2281-5.
55. Kus JV, Zaton K, Sarkar R, Cameron RK. Age-Related Resistance in Arabidopsis Is a Developmentally Regulated Defense Response to Pseudomonas syringae. The Plant Cell. 2002;14(2):479-90.
56. Krol E, Mentzel T, Chinchilla D, Boller T, Felix G, Kemmerling B, et al. Perception of the Arabidopsis Danger Signal Peptide 1 Involves the Pattern Recognition Receptor AtPEPR1 and Its Close Homologue AtPEPR2. Journal of Biological Chemistry. 2010;285(18):13471-9.
57. Yamaguchi Y, Huffaker A, Bryan AC, Tax FE, Ryan CA. PEPR2 Is a Second Receptor for the Pep1 and Pep2 Peptides and Contributes to Defense Responses in Arabidopsis. The Plant Cell. 2010;22(2):508-22.
58. Nagahara N. Intermolecular disulfide bond to modulate protein function as a redox-sensing switch. Amino Acids. 2011;41(1):59-72.
59. Liebrand TWH, Smit P, Abd-El-Haliem A, de Jonge R, Cordewener JHG, America AHP, et al. Endoplasmic Reticulum-Quality Control Chaperones Facilitate the Biogenesis of Cf Receptor-Like Proteins Involved in Pathogen Resistance of Tomato. Plant Physiology. 2012;159(4):1819-33.
60. van der Hoorn RAL, Wulff BBH, Rivas S, Durrant MC, van der Ploeg A, de Wit PJGM, et al. Structure–Function Analysis of Cf-9, a Receptor-Like Protein with Extracytoplasmic Leucine-Rich Repeats. The Plant Cell. 2005;17(3):1000-15.
61. Macho AP, Lozano-Durán R, Zipfel C. Importance of tyrosine phosphorylation in receptor kinase complexes. Trends in Plant Science. 2015;20(5):269-72.
62. Kadota Y, Shirasu K, Zipfel C. Regulation of the NADPH Oxidase RBOHD During Plant Immunity. Plant and Cell Physiology. 2015;56(8):1472-80.
63. Idänheimo N, Gauthier A, Salojärvi J, Siligato R, Brosché M, Kollist H, et al. The Arabidopsis thaliana cysteine-rich receptor-like kinases CRK6 and CRK7 protect against apoplastic oxidative stress. Biochemical and Biophysical Research Communications. 2014;445(2):457-62.
64. Tanaka H, Osakabe Y, Katsura S, Mizuno S, Maruyama K, Kusakabe K, et al. Abiotic stress-inducible receptor-like kinases negatively control ABA signaling in Arabidopsis. The Plant Journal. 2012;70(4):599-613.
65. Elmore JM, Liu J, Smith B, Phinney B, Coaker G. Quantitative Proteomics Reveals Dynamic Changes in the Plasma Membrane During Arabidopsis Immune Signaling. Molecular & Cellular Proteomics. 2012;11(4).
66. Johansson F, Olbe M, Sommarin M, Larsson C. Brij 58, a polyoxyethylene acyl ether, creates membrane vesicles of uniform sidedness. A new tool to obtain inside-out (cytoplasmic side-out) plasma membrane vesicles. The Plant Journal. 1995;7(1):165-73.
67. Shevchenko A, Tomas H, Havlis J, Olsen JV, Mann M. In-gel digestion for mass spectrometric characterization of proteins and proteomes. Nat Protocols. 2007;1(6):2856-60.

68. Craig R, Beavis RC. TANDEM: matching proteins with tandem mass spectra. Bioinformatics. 2004;20(9):1466-7.
69. Kall L, Storey JD, MacCoss MJ, Noble WS. Assigning significance to peptides identified by tandem mass spectrometry using decoy databases. Journal of Proteome Research. 2008;7(1):29-34.
70. Zhang Y, Wen Z, Washburn MP, Florens L. Refinements to label free proteome quantitation: how to deal with peptides shared by multiple proteins. Analytical chemistry. 2010;82(6):2272-81.
71. Larkin MA, Blackshields G, Brown NP, Chenna R, McGettigan PA, McWilliam H, et al. Clustal W and Clustal X version 2.0. Bioinformatics. 2007;23(21):2947-8.
72. Clough SJ, Bent AF. Floral dip: a simplified method forAgrobacterium-mediated transformation ofArabidopsis thaliana. The Plant Journal. 1998;16(6):735-43.
73. Liu J, Elmore JM, Fuglsang AT, Palmgren MG, Staskawicz BJ, Coaker G. RIN4 Functions with Plasma Membrane H+-ATPases to Regulate Stomatal Apertures during Pathogen Attack. PLoS Biol. 2009;7(6):e1000139.
74. Velásquez AC, Chakravarthy S, Martin GB. Virus-induced Gene Silencing (VIGS) in Nicotiana benthamiana and Tomato. Journal of Visualized Experiments : JoVE. 2009;(28), 1292.
75. Liu Y, Nakayama N, Schiff M, Litt A, Irish V, Dinesh-Kumar SP. Virus Induced Gene Silencing of a DEFICIENS Ortholog in Nicotiana Benthamiana. Plant Mol Biol. 2004;54(5):701-11.

Figure legends

Fig 1. Plasma membrane proteomics identified multiple differentially expressed RLKs upon perception of bacterial flagellin.

A) General overview of the experimental setup of the plasma membrane proteome analyses. Four-week-old *Arabidopsis* Col-0 plants grown in soil were sprayed with 10μM flg22 peptide or H_2O. Rosette leaf tissue was harvested for plasma membrane (PM) protein enrichment followed by mass spectrometry analyses at 180min and 720min. B) The number of differentially expressed proteins in particular protein families at 180min and 720min post flg22 treatment. C) Heatmap showing differentially expressed RLKs post flg22 treatment. Blue = down-regulated, yellow = up-regulated proteins and the values are log_2 fold change compared to the respective water treated sample. Left = RLK subfamily and right = gene name or gene identifier. D) An unrooted phylogenetic tree of all cysteine rich receptor like kinases (CRKs) located on chromosome 4 based on their full length amino acid sequences. The heatmap shows corresponding CRK expression patterns after pathogen and PAMP treatment. Transcript expression data were obtained from the BAR database and published microarray data. Plants

were treated with *P. syringae* pv. *tomato* (*Pst*) for 120min, 1µM flg22 for 240min, 10µM elf26 for 60min, and 1µM chitin for 30 min. The heat map was generated using Log_2 fold change compared to the respective untreated control plants.

Fig 2. Genetic investigation of CRK-mediated responses to *Pseudomonas syringae.*

A) Quantitative real-time PCR analyses of CRK28 and CRK29 transcripts after treatment with the bacterial elicitor flg22. RQ = relative quantification. Col-0 was treated with flg22 or water and rosette leaves were collected 3hr later for RNA extraction and cDNA synthesis. Expression was normalized to the *Arabidopsis ELONGATION FACTOR* ONE ALPHA (*AT5G60390*). This experiment was repeated three times with similar results. Error bars indicate standard deviation (n=4). Statistical differences were detected by Fisher's LSD, alpha = 0.01. Asterisks indicate statistically significant difference. B) Phenotype of four-week-old VIGS-silenced *Arabidopsis* lines. *CLA1* (*Cloroplastos alterados 1*)-silenced plants were used as a control for silencing efficiency C) RT-PCR analyses of VIGS efficiency. Expression data was normalized to *Arabidopsis UBIQUITIN EXTENSION PROTEIN 1* (*AT3G52590*). Leaves of four-week-old VIGS-silenced plants were treated with or without 100 nM flg22 for 1 hr before RNA extraction and RT-PCR analyses. D) Quantification of bacterial titers in *crk29-1* plants silenced for *CRK22* and *CRK28*_three days post-syringe infiltration with *Pst* DC3000. Col-0 plants infiltrated with VIGS constructs carrying GFP were included as a control. Error bars indicate standard deviation, n = 3 and statistical differences were detected by Fisher's LSD, alpha = 0.05, letters indicate significant differences. E) Anti-FLAG immunoblot showing protein level expression of CRK28 in two lines expressing CRK28 genomic DNA (*npro:CRK28-FLAG*) (*28-1* and *28-2*) in the *crk28-1* T-DNA mutant. The bottom panel shows the membrane stained with coomassie brilliant

blue (CBB) to show protein loading. F) Quantitative real-time PCR analyses of CRK28 expression in Col-0, *28-1* and *28-2*. RQ = relative quantification. Data were analyzed as described in (A). G) Increased expression of CRK28 enhances *Arabidopsis* resistance to *P. syringae* pv. *tomato* (*Pst)* strain DC3000. Four-week-old Col-0 and *npro:CRK28-FLAG* expression lines were syringe infiltrated with CFU/mL *Pst* DC3000 and leaves were photographed four days post-infiltration (dpi). H) Bacterial titers in Col-0 and *npro:CRK28-FLAG* expression lines four days post syringae infiltration with *Pst* DC3000. Error bars indicate standard error, n = 6. Statistical differences were detected by Fisher's LSD, alpha = 0.01 and letters indicate significant differences.

Fig 3. CRK28's extracellular cysteine residues are required for cell death induction in *Nicotiana benthamiana*.

A) Diagram showing the general domain architecture of *Arabidopsis* CRK28. The N terminus includes a secretion signal with two predicted extracellular DUF26 domains (orange) and an intracellular kinase domain (brown). Predicted extracellular cysteine residues and sub-domains important for ATP binding and activity in other kinases are highlighted. TM = transmembrane. Numbers correspond to amino acid residues. B) Cell death induced by transient expression of CRK13, CRK28, and CRK29 in *N. benthamiana. Agrobacterium* containing *35S:CRK13-FLAG, 35S:CRK28-FLAG*, *35S:CRK29-FLAG* and *35S:GFP* were infiltrated into *N. benthamiana* leaves and photographed 48 hours post-infiltration (hpi). C) Anti-FLAG immunoblot showing the expression of CRK13, CRK28, CRK29, and GFP 24hpi in *N. benthamiana*. The lower panel represents coomassie brilliant blue (CBB) stain to show protein loading. Asterisk shows an anti-FLAG cross reacting band. D) Transient expression of *35S:CRK28-FLAG* and four cysteine

mutants (C99A, C127A, C214A and C242A) in *N. benthamiana*. Cell death was observed for wild-type CRK28 whereas no cell death was observed for cysteine mutants. The leaf was photographed 48hpi. E) Anti-FLAG immunoblot demonstrating the expression of CRK28 and the cysteine mutants 20hpi. NB = *N. benthamiana* (uninfiltrated). F) *35S:CRK28-FLAG* was transiently expressed in *N. benthamiana* and the detergent soluble supernatant was used for PNGase F and EndoHf enzymatic deglycosylation assays. Although the predicted molecular weight of CRK28 is 74.46kDa, on SDS PAGE it is detected at 100kDa. G) Anti-HRP immunoblot demonstrating that CRK28 carries the complex N-linked glycan β (1,2)-xylose or α (1,3)-fucose. *35S:CRK28-FLAG* and *35S:CRK28^{K377N}-FLAG* were transiently expressed in *N. benthamiana* and subjected to anti-FLAG IP. Mature glycosylation (in the golgi) was detected using anti-HRP antibody as previously described (59). Anti-FLAG immunoblot was performed to show the amount of IP loaded.

Fig 4. The CRK28 intracellular ATP binding lysine (K377) residue is required for CRK28-mediated function and CRK28 is phosphorylated *in planta*

A) Transient expression of *35S:CRK28-FLAG, 35S:CRK28^{K377N}-FLAG, and 35S:GFP* in *N. benthamiana*. No cell death was observed for the K377N mutant. The leaf was photographed 48hpi. B) Anti-FLAG immunoblot demonstrating the expression of CRK28 and CRK28^{K377N} 20hpi. Asterisk shows an anti-FLAG cross reacting band. The bottom panel shows the membrane stained with coomassie brilliant blue (CBB) to show protein loading. C) *In planta* phosphorylation of CRK28 and CRK28^{K377N}. *35S:CRK28-FLAG*, *35S:CRK28^{K377N}-FLAG* and *35S:GFP* were transiently expressed in *N. benthamiana* and subjected to anti-FLAG immunoprecipitation. Twenty µl of the re-suspended beads were used for a kinase reaction

containing 100µM ATP. After incubating the reaction at 30ºC for 1h, the proteins were separated on SDS-PAGE and immunoblotted with anti-phospho-threonine antibody and anti-FLAG antibody. D) Overexpression of CRK28 in *Arabidopsis* affects flowering and silique development. *35S:CRK28-FLAG* and *35S:CRK28^{K377N}-FLAG* constructs were transformed into Col-0. Transgenic T1 seeds were selected on Kanamycin plates and transformants were transferred into soil along with Col-0 grown on MS plates without Kanamycin. Representative picture of transgenic T1 plants expressing *35S:CRK28-FLAG* and *35S:CRK28^{K377N}-FLAG* seven weeks post-transplanting onto soil. The same Col-0 plant was used in both pictures as the T1 plants were transplanted at the same time and grown in the same conditions. E) Anti-FLAG immunoblots showing the protein level expression of *CRK28-FLAG* and *35S:CRK28^{K377N}-FLAG*. The bottom panel shows coomassie brilliant blue (CBB) stain indicating total protein loading.

Fig 5. CRK28 expression is induced in response to flg22 and heighted expression of CRK28 enhances flg22-triggered ROS burst.

A) Quantitative real-time PCR analyses of CRK28 expression in response to treatment with flg22. Four-week-old Col-0, *npro:CRK28-FLAG* lines 28-1, and 28-2 were treated with 10µM flg22 or water (+0.025% Silwet L-77) and leaf samples were collected for RNA extraction at the indicated time points. Expression was normalized to the *Arabidopsis ELONGATION FACTOR 1-ALPHA*. RQ = relative quantification. Error bars indicate standard error, n = 3. Statistical differences were detected by Fisher's LSD, alpha = 0.05 and different letters indicate statistical significance. The experiment was repeated twice with similar results. B and C) show the ROS burst in Col-0, 28-1 and 28-2 after treatment with 100nM flg22 and 50µg/mL chitin, respectively. ROS was quantified using a luminol based assay. The graph depicts total relative light units

(RLU) detected over a 30 min period. Error bars indicate standard error, n = 16. Statistical differences were detected by Fisher's LSD, alpha=0.05. These experiments were repeated three times with similar results. D) MAPK3/6 activation assay in Col-0 and 28-2 after flg22 or water treatment. Three-week old plants were sprayed with 10μm flg22 or water (+0.025% Silwett L-77) and tissues were collected at indicated time points and processed. Phosphorylated MAPK3 and MAPK6 were detected with anti-p44/42 MAPK antibody. The bottom two panels show membranes stained with coomassie brilliant blue (CBB) to show protein loading. These experiments were repeated three times with similar results.

Fig 6. BAK1 associates with CRK28 in *Arabidopsis* and *Nicotiana benthamiana* and silencing *NbSerk3* reduces CRK28-mediated cell death.

A) CRK28 Co-IPs with BAK1 in *N. benthamiana*. *35S:CRK28-FLAG* and *35S:AtBAK1-HA* were co-expressed in *N. benthamiana* and subjected to anti-HA IP. Proteins were then subjected to anti-HA and anti-FLAG immunoblotting. B) CRK28 co-immunoprecipitates (Co-IPs) with BAK1 in *Arabidopsis*. Col-0 and the *npro*:*CRK28-FLAG* expression line 28-2 were sprayed with 10μM flg22 or water (+0.025% Silwett L-77) and subjected to anti-BAK1 IP. Proteins were separated by SDS-PAGE and immunoblotted with anti-BAK1 and anti-FLAG antibodies. C) CRK28 and CRK28^{K377N} associate with the FLS2/BAK1 immune complex in *N. benthamiana*. *35S:FLS2-GFP, 35S:BAK1-HA* and *35S:CRK28-FLAG* or *35S:CRK28^{K377N}-FLAG* were co-expressed in *N. benthamiana* and subjected to anti-GFP IP. Proteins were then subjected to anti-GFP, FLAG, and HA immunoblotting. Asterisk shows an anti-FLAG cross reacting band. D) Shows CRK28-mediated cell death in *NbSerk3* silenced and control plants (upper panel) and trypan blue staining of dead tissue (lower panel). The table represents the number of leaves that

showed weak or strong cell death (CD) per total number of leaves infiltrated. The leaf image with CRK28-FLAG expression after *NbSerk3* silencing is representative of the weak cell death observed. E) Reverse transcriptase PCR showing the expression of *NbSerk3* and *NbSerk2* in silenced plants three weeks post-infiltration with VIGS constructs. The *N. benthamiana ELONGATION FACTOR ONE ALPHA* (*NbEF-1a*) was used as an endogenous control. DCC = DNA contamination control, NTC = no template control. All experiments were repeated at least three times with similar results.

Fig 7. CRK28 self-associates in *Nicotiana benthamiana* and also associates with CRK29. A) Immunoblot showing the Co-IP of CRK28-HA with CRK28-FLAG in the presence or absence of 1μM flg22. 35S:CRK28-HA and 35S:CRK28-FLAG were co-infiltrated into *N. benthamiana* leaves and 24hpi, the leaves were infiltrated with either 1μM flg22 or water and leaf samples were collected 5 min later for immunoprecipitation. Asterisk shows an anti-FLAG cross reacting band. B) Co-IP of CRK28-HA along with CRK29-FLAG in *N. benthamiana*. The experiments were performed as described in (A). An anti-FLAG cross-reacting band is present in the first and fifth lanes. These experiments were repeated three times with similar results.

Supporting Information

S1 Table. Tandem mass spectrometry spectral count data and differential expression analyses. Columns include spectral count data that was included in differential expression analyses with QPROT and EDGE R. The worksheet S1 Table Legend provides a description of the information in each column.

S2 Table. Sequences of primers used in the manuscript.

S1 Fig. Relative abundance of LRR-RLKs in plasma membrane enriched fractions.

Left: Phylogenetic tree of all TAIR10 annotated LRR-RLKs generated from kinase domain amino acid alignments. RLK subfamily membership is indicated after the Arabidopsis Gene Identifier on the tree. Major subfamily clades are indicated in orange. Middle: Heatmap of protein differential abundance 180 and 720 minutes after FLS2 activation. Non-significant fold changes were set to zero on the $\log_2$ scale. LRR-RLKs that were not identified are indicated in black. Right: Bar chart of LRR-RLK relative protein abundance (normalized spectral abundance factors, NSAF) in water- and flg22-treated tissue 720min after treatment. Error bars represent standard deviation. Specific RLKs or RLK families are indicated in black. Note modified scale to highlight differences in lower abundance proteins. PM = plasma membrane.

S2 Fig. Relative abundance of non-LRR-RLKs in plasma membrane enriched fractions.

Left: Phylogenetic tree of all TAIR10 annotated non-LRR-RLKs generated from kinase domain amino acid alignments. RLK subfamily membership is indicated after the Arabidopsis Gene Identifier on the tree. Major subfamily clades are indicated in orange. Middle: Heatmap of protein differential abundance 180 and 720 minutes after FLS2 activation. Nonsignificant fold changes were set to zero on the $\log_2$ scale. RLKs that were not identified are indicated in black. Right: Bar chart of RLK relative protein abundance (normalized spectral abundance factors, NSAF) in water- and flg22-treated tissue 720 minutes after treatment. Error bars represent

standard deviation. Specific RLKs or RLK families are indicated in black. Note modified scale to highlight differences in lower abundance proteins. PM = plasma membrane.

S3 Fig. The chromosomal location of CRKs in *Arabidopsis* genome. The majority of the *Arabidopsis* CRKs are tandemly located on chromosome 4.

S4 Fig. Genotyping and disease phenotyping of *CRK28* and *CRK29* T-DNA knockout lines. . A) Schematic representation showing the position of the T-DNA insertion sites in *CRK28* and *CRK29*. B) RT-PCR showing the expression of *CRK28* and *CRK29* in their respective T-DNA lines compared to Col-0. Primer pairs flanking the insertion site were used for RT-PCR. The *Arabidopsis Actin 2 (ACT2)* gene was used as an endogenous control. DCC = DNA contamination control, NTC = no template control. D and E) Quantification of the *Pst DC3000* (D) and *Pst DC3000* Δ*hrcC* (E) in the wild type Col-0, *crk28-1*, and *crk29-1* plants four days post-infiltration and spray inoculation, respectively.. Error bars indicate standard deviation, n = 6. No statistically significant differences were observed between the T-DNA knockouts and Col-0. F) Quantification of *Pst DC3000* in Col-0, *crk28-1* and *crk29-1* 2dpi. For the flg22 protection assay, leaves were infiltrated with 1μM flg22 and 24h later, the same leaves were infiltrated with *Pst DC3000* ($1x10^5$ CFU/mL). Error bars indicate standard deviation, n = 8. These assay were repeated at least three times with similar results. No statistically significant differences in flg22 protection were observed between the T-DNA knockouts and Col-0.

S5 Fig. CRK28's cDNA sequence from Col-0.

CRK28 possesses seven exons and six introns. Nucleotides with blue and red font colors show the fourth and fifth exons, respectively.

S6 Fig. *In vitro* CRK28 kinase activity assay. CRK28's kinase domain purified from *E. coli* shows neither autophosphorylation nor transphosphorylation of the artificial kinase substrate myelin basic protein (MyBP). Three µg of CRK28's purified recombinant kinase domain and the kinase dead variant ($CRK28^{K377N}$) were mixed with the kinase substrate myelin basic protein (MyBP) and subjected to a kinase activity assay. The RIPK (AT2G05940) kinase was included as a positive control. The reaction was separated by SDS-PAGE and immunoblotted with anti-phospho-threonine antibody. A radioactive (^{32}P) kinase activity assay was also performed as described in (Lin et al., 2015). The bottom panel shows coomassie brilliant blue (CBB) stain showing total loaded protein.

S7 Fig. Silencing *NbSerk3* does not inhibit cell death elicited by the resistance protein RPS2. A) Anti-FLAG immunoblot detecting CRK28-FLAG and 35S:CBL-GFP-FLAG expression in silenced plants. The bottom panel is a gel stained with coomassie brilliant blue (CBB) to show protein loading. B) The cell death phenotype caused by infiltration with *CRK28*-FLAG and *RPS2-FLAG* in *NbSerk3* silenced and *TRV:GUS* infiltrated *N. benthamiana* plants. The numbers below the picture represent the number of leaves that showed weak or strong cell death per total number of leaves infiltrated. These experiments were repeated at three times with similar results. C) Anti-FLAG immunoblot verifying the expression of CRK28-FLAG and RPS2-FLAG in silenced and control plants at 20hpi. CBB = coomassie brilliant blue.

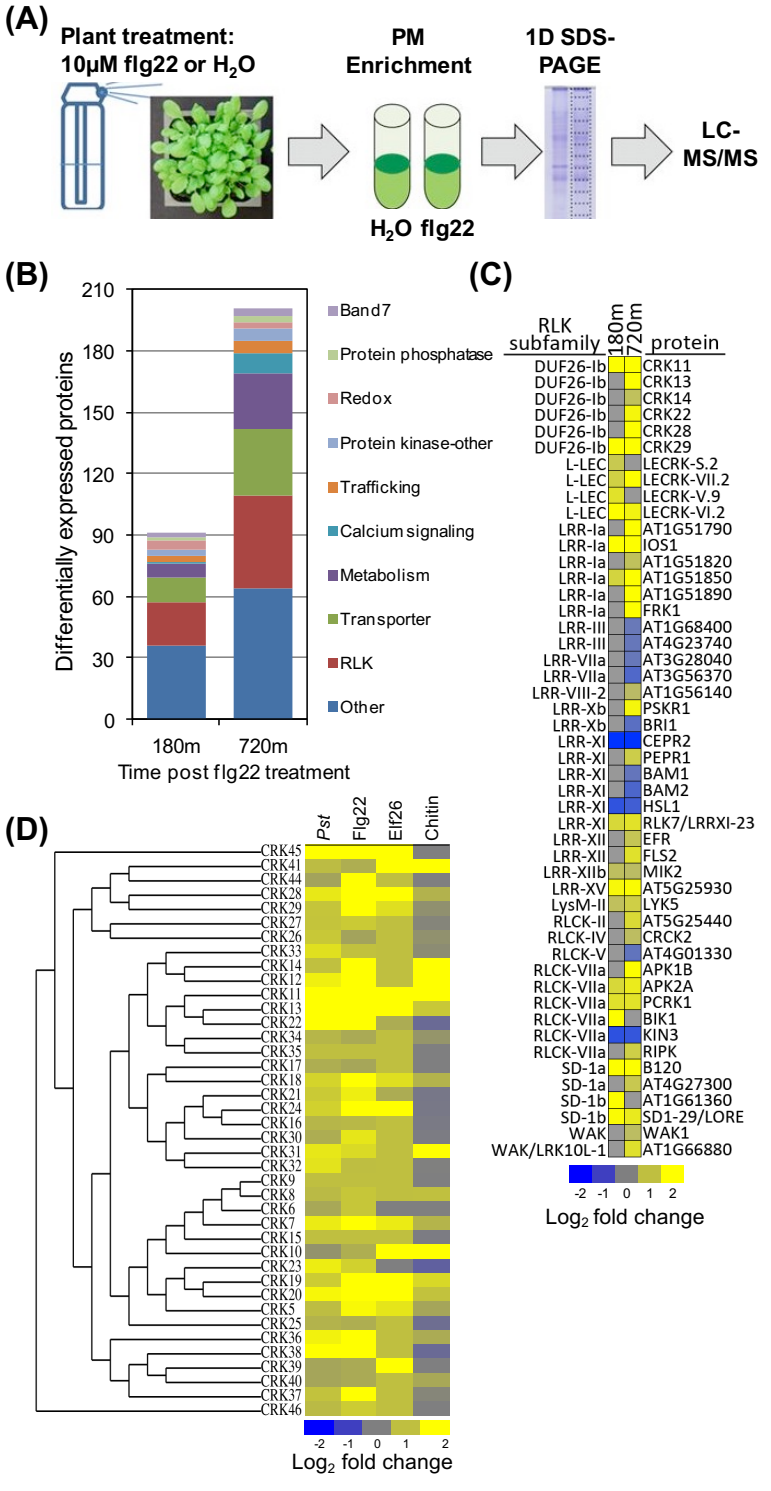
(A)
Plant treatment:
10μM flg22 or H2O
PM
Enrichment
1D SDS-
PAGE
LC-
MS/MS
H2O flg22
(B)
Differentially expressed proteins
Time post flg22 treatment
180m
720m
Band7
Protein phosphatase
Redox
Protein kinase-other
Trafficking
Calcium signaling
Metabolism
Transporter
RLK
Other
(C)
RLK subfamily
180m
720m
protein
Log2 fold change
(D)
Pst
Flg22
Elf26
Chitin
Log2 fold change

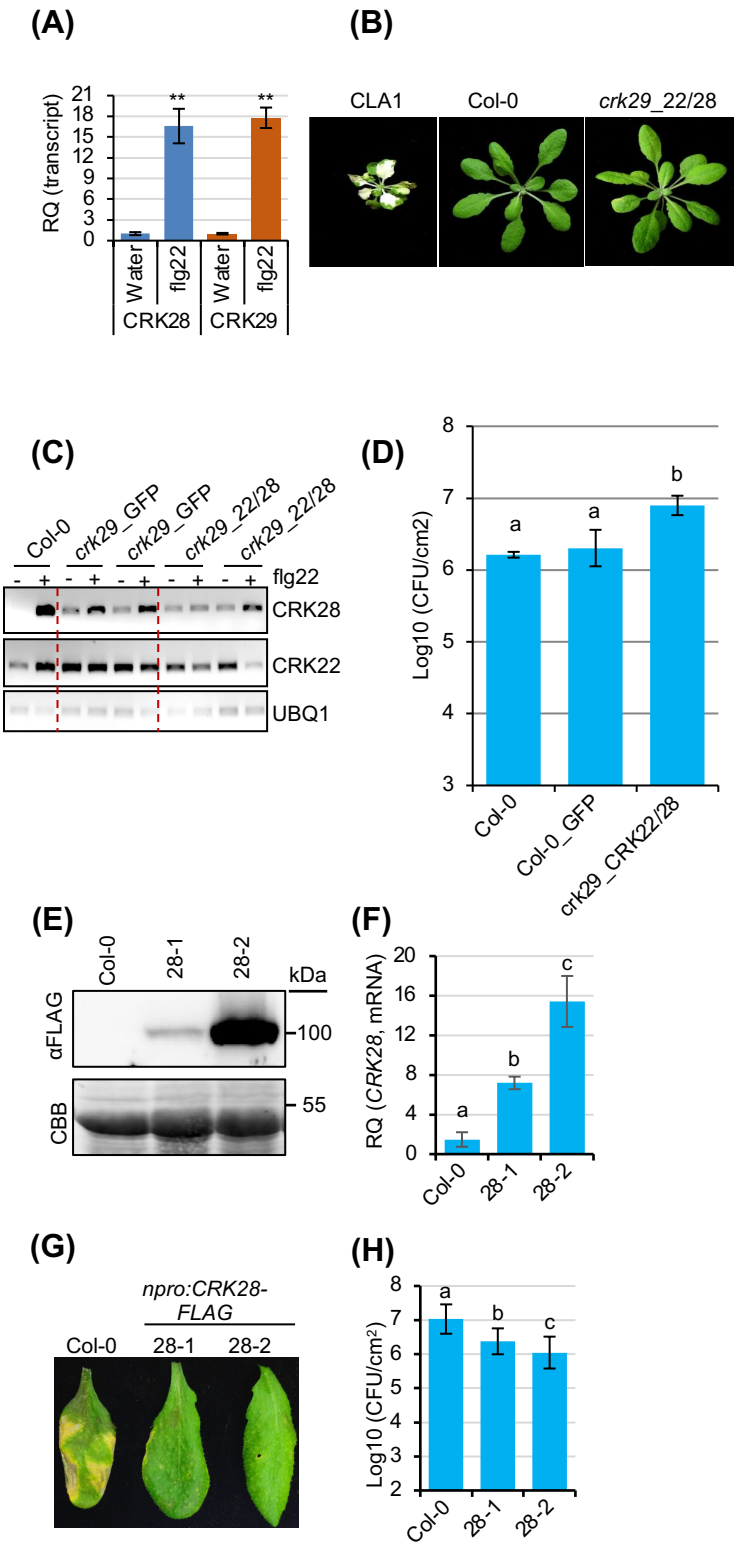
(A)
RQ (transcript)
21
18
15
12
9
6
3
0
**
**
Water
flg22
Water
flg22
CRK28
CRK29
(B)
CLA1
Col-0
crk29_22/28
(C)
Col-0
crk29_GFP
crk29_GFP
crk29_22/28
crk29_22/28
- + - + - + - + - +
flg22
CRK28
CRK22
UBQ1
(D)
Log10 (CFU/cm2)
8
7
6
5
4
3
a
a
b
Col-0
Col-0_GFP
crk29_CRK22/28
(E)
Col-0
28-1
28-2
kDa
αFLAG
100
CBB
55
(F)
RQ (CRK28, mRNA)
20
16
12
8
4
0
a
b
c
Col-0
28-1
28-2
(G)
npro:CRK28-FLAG
Col-0
28-1
28-2
(H)
Log10 (CFU/cm²)
8
7
6
5
4
3
2
a
b
c
Col-0
28-1
28-2

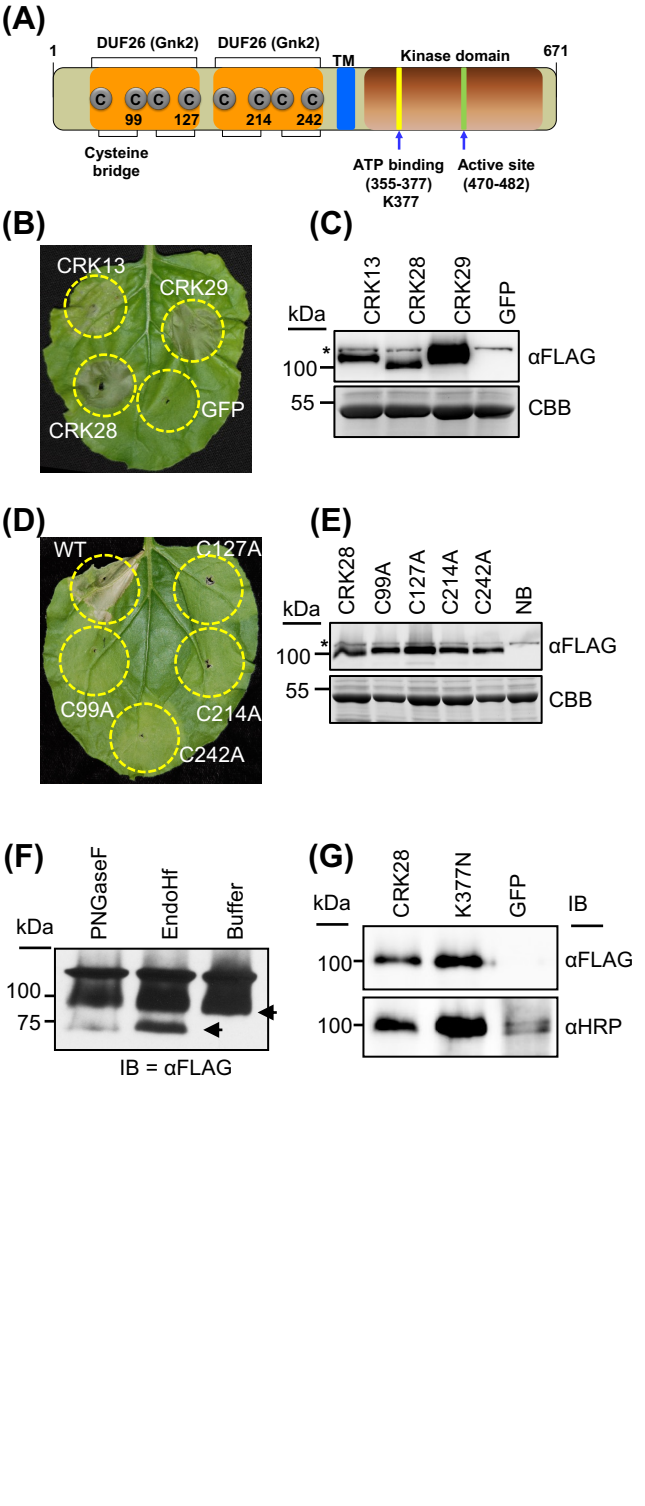
(A)
1
DUF26 (Gnk2)
DUF26 (Gnk2)
TM
Kinase domain
671
C
99
127
214
242
Cysteine bridge
ATP binding (355-377) K377
Active site (470-482)
(B)
CRK13
CRK29
GFP
CRK28
(C)
kDa
CRK13
CRK28
CRK29
GFP
100
55
αFLAG
CBB
(D)
WT
C127A
C99A
C214A
C242A
(E)
kDa
CRK28
C99A
C127A
C214A
C242A
NB
100
55
αFLAG
CBB
(F)
kDa
PNGaseF
EndoHf
Buffer
100
75
IB = αFLAG
(G)
kDa
CRK28
K377N
GFP
IB
100
100
αFLAG
αHRP

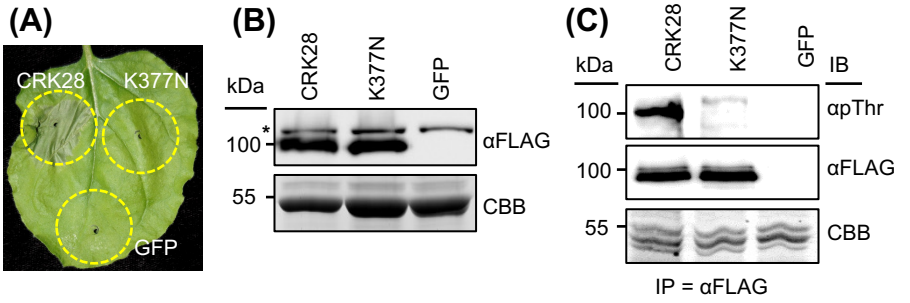
(A)
CRK28
K377N
GFP
(B)
kDa
CRK28
K377N
GFP
100
*
αFLAG
55
CBB
(C)
kDa
CRK28
K377N
GFP
IB
100
αpThr
100
αFLAG
55
CBB
IP = αFLAG

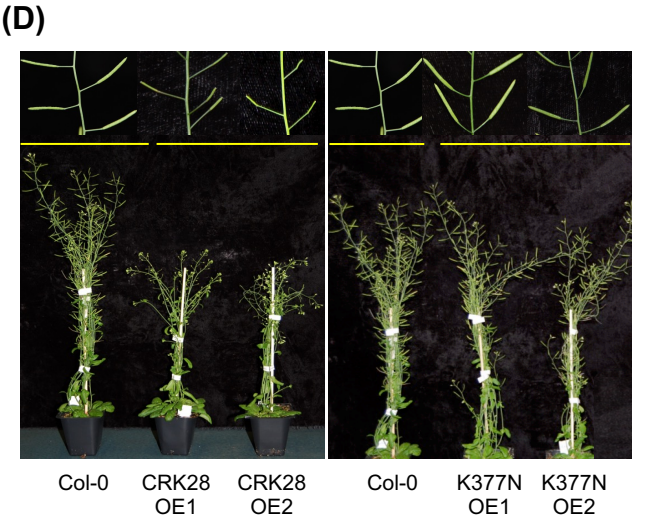
(D)
Col-0
CRK28 OE1
CRK28 OE2
Col-0
K377N OE1
K377N OE2

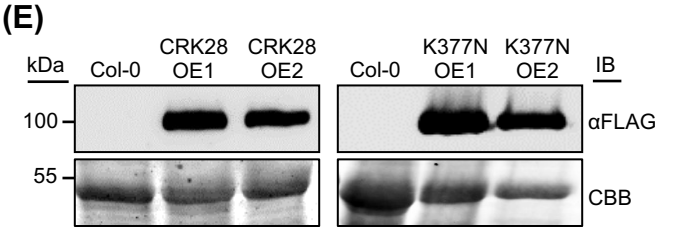
(E)
kDa
Col-0
CRK28 OE1
CRK28 OE2
Col-0
K377N OE1
K377N OE2
IB
100
αFLAG
55
CBB

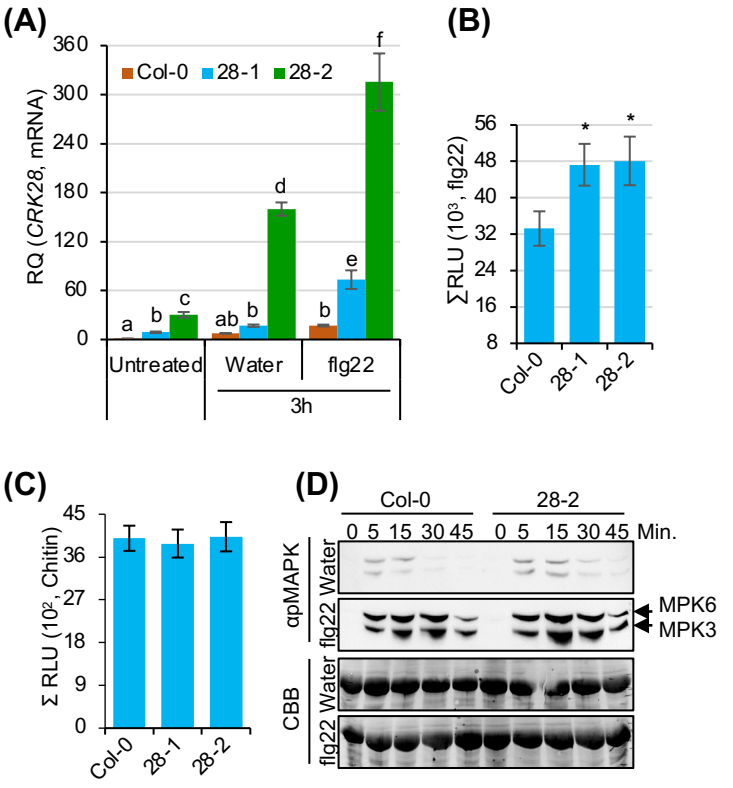
(A)
RQ (CRK28, mRNA)
360
300
240
180
120
60
0
Col-0
28-1
28-2
a
b
c
ab
b
d
b
e
f
Untreated
Water
flg22
3h
(B)
ΣRLU (10³, flg22)
56
48
40
32
24
16
8
*
*
Col-0
28-1
28-2
(C)
Σ RLU (10², Chitin)
45
36
27
18
9
0
Col-0
28-1
28-2
(D)
Col-0
28-2
0 5 15 30 45 0 5 15 30 45 Min.
αpMAPK
Water
flg22
MPK6
MPK3
CBB
Water
flg22

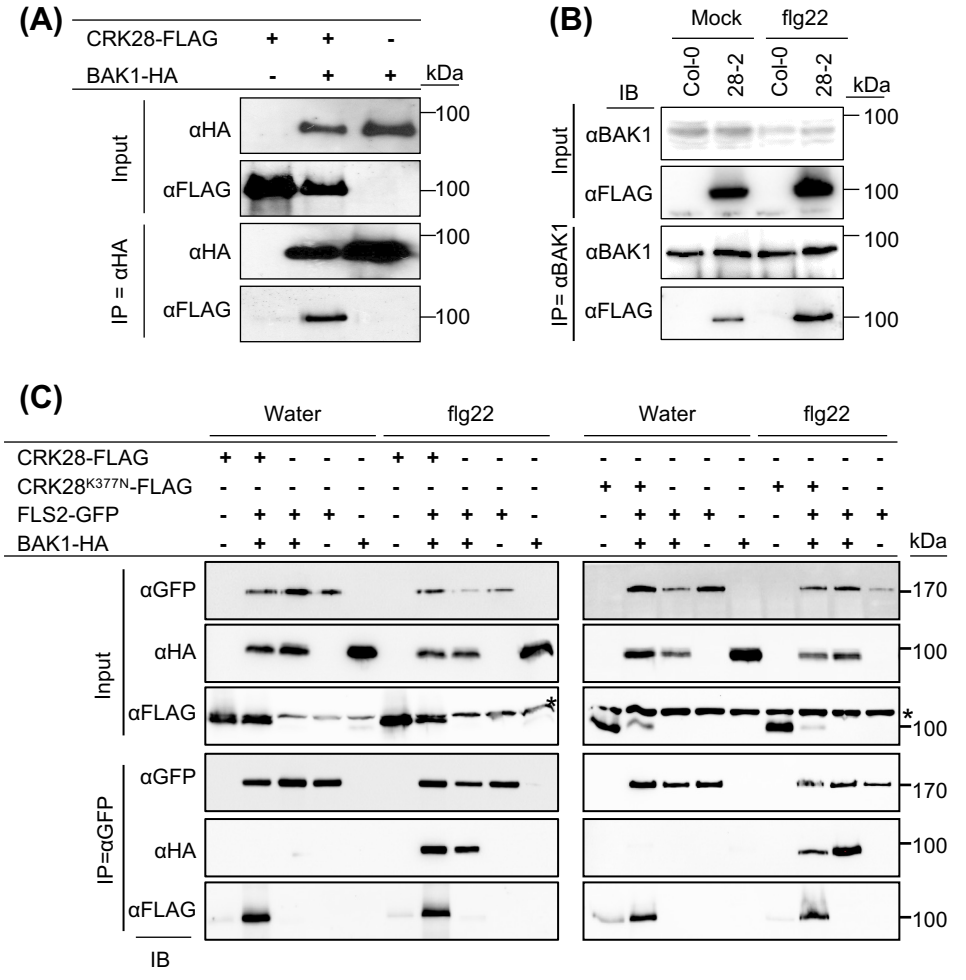
(A)
CRK28-FLAG + + -
BAK1-HA - + +
kDa
Input
αHA
αFLAG
IP = αHA
αHA
αFLAG
100
100
100
100
(B)
Mock
flg22
Col-0
28-2
Col-0
28-2
IB
kDa
Input
αBAK1
αFLAG
IP= αBAK1
αBAK1
αFLAG
100
100
100
100
(C)
Water
flg22
Water
flg22
CRK28-FLAG + + - - - + + - - -
CRK28K377N-FLAG - - - - - - - - - -
FLS2-GFP - + + + - - + + + -
BAK1-HA - + + - + - + + - +
CRK28-FLAG - - - - - + + - - -
CRK28K377N-FLAG + + - - - + + - - -
FLS2-GFP - + + + - - + + + -
BAK1-HA - + + - + - + + - +
kDa
Input
αGFP
αHA
αFLAG
IP=αGFP
αGFP
αHA
αFLAG
IB
170
100
100
170
100
100
(D)
TRV: NbSERK3
TRV:GUS
CRK28-FLAG
GFP-FLAG
CRK28-FLAG
GFP-FLAG
Weak CD 6 0 0 0
Strong CD 0 0 11 0
#Total 11 11 11 11
(E)
Ladder
TRV: GUS
TRV: NbSerk3
DCC
NTC
NbSerk3
NbSerk2
NbEF-1a

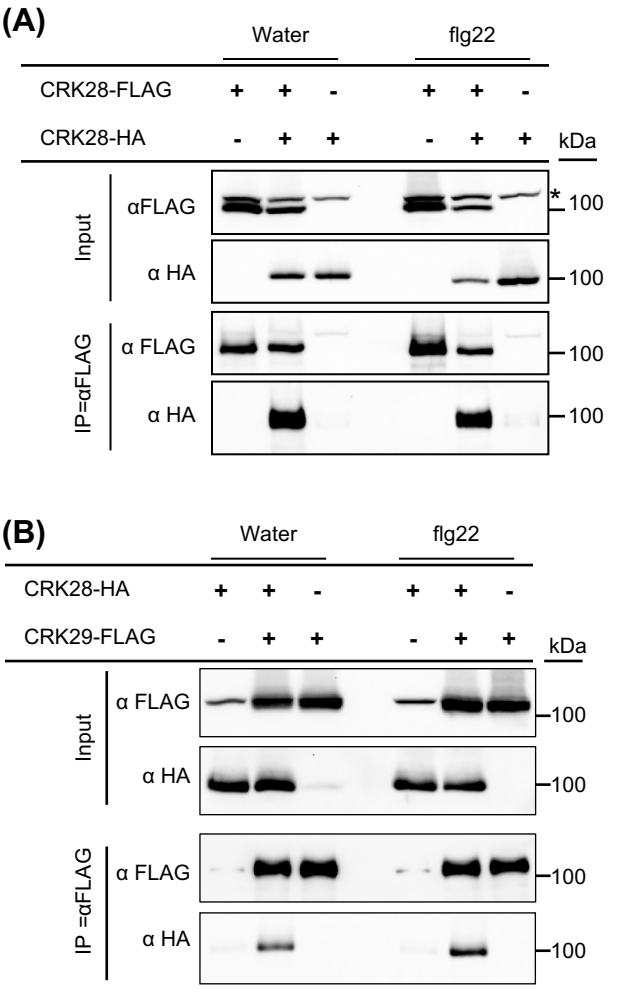
(A)
Water
flg22
CRK28-FLAG
+ + - + + -
CRK28-HA
- + + - + +
kDa
Input
αFLAG
α HA
IP=αFLAG
α FLAG
α HA
*
100
100
100
100
(B)
Water
flg22
CRK28-HA
+ + - + + -
CRK29-FLAG
- + + - + +
kDa
Input
α FLAG
α HA
IP =αFLAG
α FLAG
α HA
100
100
100
100